DISSERTATIONES CHIMICAE UNIVERSITATIS TARTUENSIS
75

DISSERTATIONES CHIMICAE UNIVERSITATIS TARTUENSIS
75

PRIIT MÖLLER

Electrochemical characteristics of some cathodes for medium temperature solid oxide fuel cells, synthesized by solid state reaction technique

TARTU UNIVERSITY
PRESS

Institute of Chemistry, University of Tartu, Estonia

Dissertation is accepted for the commencement of the degree of Doctor of Philosophy in Chemistry on April 24, 2008, by the Doctoral Committee of the Institute of Chemistry, University of Tartu.

Supervisor: Prof. Enn Lust, University of Tartu, Estonia

Opponents: Dr. Peter Holtappels, EMPA (Swiss Federal Laboratories for Materials Testing and Research), Switzerland

Prof. Enn Mellikov, Tallinn University of Technology, Estonia

Commencement: 11^{00} June 18, 2008, in Tartu, 18 Ülikooli Str., in the University council hall

ISSN 1406–0299
ISBN 978–9949–11–874–8 (trükis)
ISBN 978–9949–11–875–5 (PDF)

Tartu Ülikooli Kirjastus
www.tyk.ee
Tellimus nr 183

to my parents

CONTENTS

1. LIST OF ORIGINAL PUBLICATIONS

I E. Lust, **P. Möller**, I. Kivi, G. Nurk, S. Kallip, P. Nigu, K. Lust, Optimization of the cathode composition for the intermediate-temperature SOFC. Journal of the Electrochemical Society, 152 (2005) A2306–A2308.

II E. Lust, G. Nurk, S. Kallip, I. Kivi, **P. Möller**, Electrochemical characteristics of $Ce_{0.8}Gd_{0.2}O_{1.9}|La_{0.6}Sr_{0.4}CoO_{3-\delta}$ + $Ce_{0.8}Gd_{0.2}O_{1.9}$ half-cell. Journal of Solid State Electrochemistry, 9 (2005) 674–683.

III E. Lust, **P. Möller**, I. Kivi, G. Nurk, S. Kallip, Electrochemical characteristics of $La_{0.6}Sr_{0.4}CoO_{3-\delta}$, $Pr_{0.6}Sr_{0.4}CoO_{3-\delta}$ and $Gd_{0.6}Sr_{0.4}CoO_{3-\delta}$ on $Ce_{0.85}Sm_{0.15}O_{1.925}$ electrolyte. Journal of Solid State Electrochemistry, 9 (2005) 882–889.

IV E. Lust, G. Nurk, **P. Möller**, I. Kivi, S. Kallip, Oxygen reduction and electrochemical characteristics of half-cells for intermediate SOFCs, 26th Risø International Symposium on Materials Science, Risø, 2005, 279–284.

Author's contribution:

Performed the cathode and electrolyte materials preparations, electrochemical measurements, modelling and interpretations [I, II].

Participated in the cathode and electrolyte materials preparations, electrochemical measurements, modelling, interpretations [III, IV] and participated in preparation of all manuscripts [I–IV].

2. ABBREVIATIONS AND SYMBOLS

A	CPE coefficient
A_D	activation energy, obtained from the diffusion resistance R_D vs. temperature plots
AFM	atomic force microscopy
BET	Brunauer, Emmett and Teller method
c_0	interfacial oxygen ion vacancy concentration
C_1	medium frequency capacitance
C_2	low frequency capacitance
C_{gb}	grain boundary capacitance
CGO	$Ce_{1-x}Gd_xO_{2-\delta}$
CPE_1	high-frequency constant phase element
CPE_2	low- frequency constant phase element
CSO	$Ce_{1-x}Sm_xO_{2-\delta}$
D	diffusion coefficient
E	electrode potential
E'	working electrode potential
E_{act}	activation energy, obtained from Z',Z'-plots
E_{OCV}	open-circuit potential
f	ac frequency
F	Faraday' constant
FC	fuel cell
GFW	generalized finite Warburg element
GSCO	$Gd_{1-x}Sr_xCoO_{3-\delta}$
j	current density
j_0	exchange current density
j_c	cathodic current density
L	effective diffusion layer thickness
LSCFO	$La_{1-x}Sr_xCo_{1-y}Fe_yO_{3-\delta}$
LSCO	$La_{1-x}Sr_xCoO_{3-\delta}$
LSMO	$La_{1-x}Sr_xMnO_{3-\delta}$
n	number of electrons transferred
p_{O2}	oxygen pressure
PSCO	$Pr_{1-x}Sr_xCoO_{3-\delta}$
R	universal gas constant
R_1	high-frequency charge transfer resistance
R_2	low- frequency charge transfer resistance
R_{AFM}	AFM surface roughness
R_D	diffusion resistance
R_{ex}	total very high frequency series resistance
R_{gb}	grain boundary resistance
R_{LF}	low-frequency polarisation resistance
R_{MF}	medium-frequency polarisation resistance

R_{ms}	AFM root mean square height
R_p	total polarization resistance
S_{AFM}	surface area of a material obtained by using AFM method
S_{BET}	specific surface area, obtained by the BET method
S_{el}	surface area of electrode
SEM	scanning electron microscopy
SOFC	solid oxide fuel cell
T	temperature
t	time
TEC	thermal expansion coefficient
TPB	three-phase boundary
T_W	GFW frequency parameter ($T_W = L^2 D^{-1}$)
YSZ	yttria stabilised zirconia
Z_W	Warburg-like diffusion impedance
α	CPE fractional exponent
α_a	transfer coefficient for the anode (oxidation) reaction
α_c	transfer coefficient for cathode (reduction) reaction
α_w	GFW fractional exponent
σ_e	electronic conductivity
σ_{ox}	oxygen ion conductivity
δ	phase angle
τ_{max}	characteristic relation time
Δ^2	weighted sum of the squares
χ^2	chi-square function
η	overpotential
η_c	cathodic overpotential
ω	angular frequency (equal to $2\pi f$)

3. INTRODUCTION

Fuel cells (FC) are the modern electrochemical devices that convert the chemical energy of a fuel into the electric energy and heat energy with the very high efficiency from 40 to 80% depending no the working temperature and fuel used. FC single cell consists of the compact of porous cathode (where oxygen reduction process occurs) and porous anode (where oxidation of fuel takes place) and a compact homogenous electrolyte layer between cathode and anode. In a typical fuel cell fuels in gaseous phase (typically hydrogen, methane, methanol, ethanol etc) are continuously fed to the anode compartment and an oxidant (typically oxygen from air or pure oxygen) is continuously fed to the cathode compartment. The electrochemical redox reactions takes place at porous structure of electrodes to produce an electric current and residual heat, because the exothermic fuel oxidation reaction occurs. A clean water is final product if hydrogen is used as fuel. It should be noted that the chemical energy conversation efficiency increases with the rise of working temperature and for solid oxide fuel cells (SOFCs) it is as high as 60÷70%. Therefore the SOFCs are very attractive systems taking into account that the various hydrogen containing compounds (natural gas, various alkanes, diesel, gasoline, alcohols, esters, H_2S, NH_3, wood gas etc) can be used as fuels.

Solid oxide fuel cells operating at intermediate temperatures (from 750 to 1000 K) have received considerable attention for use in the direct conversation of chemical energy of a fuel into the electrical and heat energies because the high-temperature corrosion problems are not so critical as for SOFCs operating at $T > 1000$K. Thus for construction of the intermediate temperature SOFCs less expensive construction materials can be used.

In many papers the ceria based solid solutions ($Ce_{1-x}Gd_xO_{2-\delta}$, $Ce_{1-x}Sm_xO_{2-\delta}$) have been pointed out as the most promising electrolytes for intermediate temperature SOFCs, having noticeably higher oxygen ion conductivity, i.e. the lower series resistance values at $T \leq 973$ K than yttria stabilised zirconia (YSZ) based SOFCs. However, the electrochemical behaviour of interfaces between porous $La_{0.6}Sr_{0.4}CoO_{3-\delta}$ (LSCO), $Pr_{0.6}Sr_{0.4}CoO_{3-\delta}$ (PSCO) or $Gd_{0.6}Sr_{0.4}CoO_{3-\delta}$ (GSCO) and B-site substituted $La_{1-x}Sr_xCo_{1-y}Fe_yO_{3-\delta}$ (LSCFO), as well as mixed with various electrolytes LSCO or LSCFO (for example $La_{0.6}Sr_{0.4}Co_{0.2}Fe_{0.8}O_{3-\delta}$ + $Ce_{0.9}Gd_{0.1}O_{2-\delta}$) is an open question. It should be noted that the addition of Fe^{3+} ions into the B-site of cathode (partial replacement of Co^{3+} with Fe^{3+} cations) as well as electrolyte into the single phase cathode decreases the thermal expansion coefficient of the cathode. However, these additions decrease the cathodic catalytic activity of oxygen electroreduction as well and thus the detailed studies are inevitable to optimize the cathode chemical composition.

The main aim of this work was to synthesize $La_{0.6}Sr_{0.4}CoO_{3-\delta}$, $Pr_{0.6}Sr_{0.4}CoO_{3-\delta}$ and $Gd_{0.6}Sr_{0.4}CoO_{3-\delta}$ cathode materials and to obtain the electrochemical characteristics of the half-cells with various cathode and

electrolyte compositions to establish the nature of the limiting stages for oxygen electroreduction in solid oxide fuel cells. As important part of the work the operation time stability tests of various half-cells was made as the time stability during the long operation times of the materials used are essential for development of solid oxide fuel cells.

4. LITERATURE OVERVIEW

4.1. Influence of the cathode and electrolyte composition on the electrochemical characteristic properties of half-cells for SOFCs

Lowering of the operating temperature to an intermediate temperature region of 750–1000 K is the main challenge in current SOFC research activities. Such a reduction would greatly enhance the long-term performance stability, widen the material selection, lessen the sealing problem and enables the use of low-cost metallic interconnects [1–7]. However, it should be noted that the performance of the intermediate temperature SOFCs strongly depends on the characteristics of the cathode as well as on the properties of the cathode | electrolyte interface since the total polarization resistance increases noticeably as temperature is decreased [8–17]. More particularly, for higher efficiency of SOFCs considerable improvements of the cathode material characteristics (catalytic activity and porosity) are inevitable because of the large cathode polarization resistance at these intermediate temperatures [2–6, 18–27].

$La_{1-x}Sr_xCoO_{3-\delta}$ (LSCO) is an excellent perovskite material for fundamental studies because it is reversibly reducible, has high rates of surface exchange and diffusion of oxygen species (diffusion coefficient $D = 4.9\times10^{-9}$ cm^2 s^{-1} in compact $La_{0.7}Sr_{0.3}CoO_{3-\delta}$ at $T = 807$ K). The interfacial oxygen ion vacancy concentration c_0 is equal to 2×10^{-4} mol cm^{-3} and c_0 decreases slightly with increasing temperature [18]. However, the thermal expansion coefficient (TEC) is very high (TEC = 21.8×10^{-6} cm K^{-1} for compact $La_{0.6}Sr_{0.4}CoO_{3-\delta}$ at $T = 873$ K) and thermal compatibility problems with ceria based electrolytes may arise during thermocycling of the cells. The substitution of the Fe^{3+} ions into the B site of $La_{1-x}Sr_xCoO_{3-\delta}$ reduces the TEC values noticeably, but the catalytic activity of $La_{1-x}Sr_xCo_{1-y}Fe_yO_{3-\delta}$ (LSCFO) is quite low [2–5,10,11]. Similarly to $La_{1-x}Sr_xMnO_{3-\delta}$ (LSMO) (with electronic conductivity $\sigma_e = 200\ldots300$ S cm^{-1} [5]), LSCFO is a very good electronic conductor ($\sigma_e = 230$ S cm^{-1}, obtained for $La_{0.6}Sr_{0.4}Co_{0.2}Fe_{0.8}O_{3-\delta}$ at $T = 900$°C), having very high oxygen diffusion coefficient and the oxygen ion conductivity σ_{ox} is ≈0.2 S cm^{-1} for $La_{0.6}Sr_{0.4}Co_{0.2}Fe_{0.8}O_{3-\delta}$ at $T = 900$°C [5,10,11]. Thus, the oxide ion conductivity in ferrites / cobaltites ($La_{1-x}Sr_xCo_{1-y}Fe_yO_{3-\delta}$) is even some orders of magnitude higher than in manganites [3,4,10,11,28], and thus LSCFO is a very good mixed conductor. The TEC value for $La_{0.6}Sr_{0.4}Co_{0.2}Fe_{0.8}O_{3-\delta}$ is 15.3×10^{-6} cm K^{-1} [10,11] which is greater than TEC for CGO electrolyte (12.5×10^{-6} cm K^{-1}). Kostogloudis and Ftikos demonstrated that the A-site deficient $La_{0.6-z}Sr_{0.4}Co_{0.2}Fe_{0.8}O_{3-\delta}$ based perovskite oxides have somewhat lower TEC values [10] than $La_{0.6}Sr_{0.4}Co_{0.2}Fe_{0.8}O_{3-\delta}$, but these materials have comparatively low time stability.

$La_{0.8}$ $Sr_{0.2}CoO_{3-\delta}$ and $La_{0.8}$ $Sr_{0.2}MnO_{3-\delta}$ cathodes, prepared by laser ablation method on a YSZ single crystal oxygen ionic conductor, have been studied by Imanishi et al. [19]. The results of impedance spectroscopy show that the dissociative adsorption of O_2 on LSCO and the charge transfer process i.e. electroreduction of O_2 on LSMO are the rate-determining steps, respectively [19]. The results of investigations for LSMO|YSZ (YSZ – yttria stabilized zirconia Y_2O_3–ZrO_2) interface demonstrate that the oxygen ion transfer across the electrode | electrolyte interface is relatively fast and unlikely to be the rate controlling stage [15]. Conventional LSMO electrodes modified by ion impregnation method (i.e. with solution of $Ce_{0.8}Gd_{0.2}(NO_3)_x$) demonstrated very good activity for O_2 electroreduction and the polarization resistance decreased to ~0.72 $\Omega\,cm^2$ as compared to 26.4 $\Omega\,cm^2$ for pure $La_{0.72}Sr_{0.18}MnO_{3-\delta}$ [20–23], however there is no results about the time stability of these materials in literature .

Barnett et al. [21,22,25] studied the influence of porosity of LSMO on the characteristics of the LSMO|YSZ interface. It was found that the cathodes with 23% and 40% total porosity show similar behavior at low current densities, but after passing a critical current density, the cell voltage dropped rapidly for the cell with lower cathode porosity, which was explained by the mass transport limitations of oxidant in the porous cathode material [25]. The results obtained by Ostergard et al. [26] show that, for the coarse-grained cathode $La_{0.85}Sr_{0.15}Mn_yO_{3-\delta}$ | YSZ, the total polarization resistance is lower than that for fine-grained LSMO.

Optimization of the double-layered $La_{0.65}Sr_{0.35}MnO_3$ | LSM+Y_2O_3 stabilized ZrO_2 (YSZ) cathode, applied on a thin YSZ layer, has been made by Haanappel et al. [27]. The influence of the LSMO|YSZ mass ratio of the cathode functional layer, the grain size of LSMO powder for the cathode current collector layer, thickness of the cathode functional layer and cathode current collector layer as well as influence of calcinations temperature and durability of the YSZ powder, used for preparation of the cathode functional layer, were analyzed in detail [27]. The chemical degradation of the $La_{1-x}Sr_xMnO_3$ | Y_2O_3 stabilized ZrO_2 composite cathodes in the presence of current collector pastes (Bi containing Pt-paste for example) was studied by Chervin et al. [29]. Bi containing Pt-paste reacted with the composite cathode at $T > 800$°C, which after various complicated surface reactions led to formation of the phyroclore phase, $La_2Zr_2O_7$ at Y_2O_3 – ZrO_2 surface. Influence of the electrode polarization on the oxygen nonstoichiometry on the $La_{0.9}Sr_{0.1}MnO_{3+\delta}$ | YSZ interface has been studied by Yasumoto et al. [24] at $873 < T < 1273$ K. It was found that the oxygen nonstoichiometry affects the cathode reactivity through the exchange current density.

Ringuede and Fouletier [16] established that in air at moderate temperature $T < 803$ K the electrode reaction at $La_{0.7}Sr_{0.3}CoO_{3-\delta}$ was controlled by the oxygen diffusion rate through the dense LSCO layer according to the internal

diffusion material model. The activation energy for diffusion process obtained using Warburg diffusion impedance values was nearly 1.08 eV [15–18].

De Souza and Kilner [30] have shown that the activation energy is strongly dependent upon the acceptor dopant level and position, varying from ca $A_d = 3.1$ eV for undoped LCO material to $A_d \sim 1$ eV for $La_{0.4}Sr_{0.6}CoO_{3-\delta}$ [15,30]. It should be noted that the low-frequency polarization resistance (R_{LF}) increased when the oxygen pressure decreased. Although a noticeable increase of the deviation of stoichiometry was measured by thermogravimetry and it was assumed that the vacancy diffusion through the dense LSCO is rapid and the gas phase polarization becomes limiting at low O_2 pressures [15]. Under higher oxygen pressures ($p_{O_2} > 6\times10^{-3}$ bar) at $T > 773$ K the low-frequency polarization resistance was proportional to $p_{O_2}^{-0.5}$, indicating a dissociative adsorption limiting step [15] in a good agreement with experimental data for 2 μm thick dense LSCO cathode [31].

The Anderson et al. results [32] demonstrated that the dissociative adsorption at the LSCO surface is the rate-determining step at $T > 450$°C. The same conclusion has been made by Fukunaga et al. [33] for the dense LSCO and dense LSCFO cathodes working effectively at $T \geq 800$°C under high oxygen partial pressure p_{O_2}. The changes in activation energy with temperature for CGO | LSCFO interface in air (A_d is equal to 1.56 and 0.86 eV at $T > 750$ and $T < 750$°C respectively) have been calculated by Waller et al. [34]. According to Masuda et al. for dense $La_{0.6}Sr_{0.4}CoO_{3-\delta}$ cathode the values of $A_d \approx 1.1$ eV at lower $p_{O_2} < 5\cdot10^{-2}$ bar and $A_d \approx 1.5$ eV at $p_{O_2} \geq 0.1$ bar have been established at $T > 500$°C [35].

However, Adler et al. [9] have demonstrated that it is necessary to include the gas-phase diffusion term into electroreduction model at lower p_{O_2} [7] and the overall oxygen electroreduction reaction

$$0.5\ O_2 + 2e^- \rightarrow O^{2-}$$

can be simulated as a homogeneous chemical reaction occurring over the internal surface area of the porous cathode material [9]. The adsorption of neutral oxygen species by the mixed ionic conductor serves to convert electronic current to ionic current over finite region of the electrode thickness (0.5…10 μm). This active region is described by the characteristic length, related to the exchange and diffusion properties of the mixed conductor and the surface exchange reaction is limited by O_2 dissociation step rather than availability of electronic or ionic species (i.e. electron transfer step) [7]. This model also predicts that gas phase diffusion becomes dominant at very low oxygen partial pressures below 1% of O_2 in N_2 even at very small current density value i.e. near the equilibrium conditions [7].

The electrochemical properties of interfaces between porous $La_{0.6}Sr_{0.4}Co_{0.2}Fe_{0.8}O_{3-\delta}$ + $Ce_{0.9}Gd_{0.1}O_{2-\delta}$ (so-called mixed cathode) and CGO electrolyte at intermediate temperatures (500...700°C) has been investigated by Dusastre and Kilner [4] using impedance spectroscopy. The optimum CGO addition equal to 30% by weight to the LSCFO perovskite cathode resulted in four times lower area specific resistivity, but the electrochemical properties of these composites were found to be quite sensitive to the microstructure and composition of the cathode [4]. It was found that the observed high performance of the composite cathodes is consistent with the effective medium percolation theory which predicts the ambipolar transport behavior of composite mixed ionic-electronic conductors as a function of the volume fraction of each of the randomly distributed constituent phases [4,5,36,37]. However, a slight discrepancy between measurements and theory observed was explained by the fact that the overall performance of a porous electrode is not only determined by mixed conducting transport properties in the solid cathode phase but also by the inherent catalytic property of the triple phase boundary (TPB) and by the complicated mass transport of oxygen to the TPB [2–4,7].

Thus, there are actually three macroscopic pathways available for O_2 reduction process to occur on porous cathode | solid electrolyte interface and kinetics of this reaction is influenced by several factors [3,4,7,38–41]: (a) the reaction of molecular oxygen with electrolyte (CGO) surface what can be neglected at low temperature as the surface exchange coefficient is very low [4]; (b) dissociative adsorption of oxygen molecules followed by the surface diffusion step toward the three-phase boundary (TPB); and (c) surface reduction reaction followed by dissolution (adsorption/absorption) of charged oxygen species inside the cathode and masstransfer of oxygen ions toward the cathode | electrolyte boundary. It should be noted that all of these stages can be the rate-determining steps depending on T, p_{O2} and cathode polarization. However, the concentration polarization of the cathode reaction, caused by the diffusion and exchange of oxygen species to the electrode | electrolyte interface can be rate determining process at lower T [4]. The solid state mass transfer of oxygen ions includes normal bulk lattice diffusion together with contribution from the grain boundary and dislocation core pathways depending on the level of bulk diffusivity [3,4,7,9,28].

It should be noted that although there is an agreement about the possible pathways, however, there remain uncertainty and disagreement about the rate-controlling steps, explained by the difficulties in separating the relative effects of microstructure and electrocatalytic activity [40,41]. The actual role of nano, meso and macro pores in a porous electrode can be rather complicated as if there is rapid transport of electronic and ionic species along the pore surfaces due to surface diffusion, then an additional phase should be assigned to represent the surface or interfacial layer in the composite cathode [4].

The experimental results presented in Refs. [2–32] show that the activation energy of the electroreduction reaction is strongly influenced by the preparation

method for the synthesis of cathode material used, i.e. by the microscopic/ macroscopic parameters of the electrode. However, for the future development of SOFC, the time-stability tests during thousand of working hours and under the conditions of thermocycling and cathodic polarisation are inevitable.

4.2. Oxygen electroreduction mechanism at mixed conducting cathodes

The overall reaction of oxygen electroreduction to the first very simplified approximation at the SOFC cathode can be expressed as

$$0.5\mathrm{O}_2(g) + 2e^- + \mathrm{V}_\mathrm{O}^{\bullet\bullet} \rightarrow \mathrm{O}_\mathrm{O}^\mathrm{x} \qquad [4.2.1]$$

where $O_2(g)$, $V_O^{\bullet\bullet}$ and O_O^x represent an oxygen molecule in a gas phase, oxygen vacancy and an oxygen ion at a regular oxygen site, respectively [2,42]. If we, to a first approximation, assume that the relationship between the current density j and the overpotential η across the interface ($\eta = E'\text{-}E_{OCV}$, where E' is the working electrode potential and E_{OCV} is the open-circuit potential), can be described by the usual Butler – Volmer equation [42,43]

$$j = j_0\left[\exp(\alpha_\mathrm{a} nF\eta / RT) - \exp(-\alpha_\mathrm{c} nF\eta / RT)\right] \qquad [4.2.2]$$

where j_0 is the exchange current density, F is the Faraday's constant, R is the universal gas constant, n is the number of electrons transferred, and T is the absolute temperature, α_a and α_c are the transfer coefficients for the anode (oxidation) and cathode (reduction) reactions, respectively. Thus the total polarization resistance R_p can be approximated as

$$R_\mathrm{p} = \left(\frac{\partial\eta}{\partial j}\right) = \frac{RT}{nF}\left(\frac{1}{\alpha_\mathrm{a} + \alpha_\mathrm{c}}\right)\frac{1}{j_0} \qquad [4.2.3]$$

and the exchange current density at these conditions is given as

$$j_0 = \frac{RT}{nF}\left(\frac{1}{\alpha_\mathrm{a} + \alpha_\mathrm{c}}\right)\frac{1}{R_\mathrm{p}} \qquad [4.2.4]$$

At very high cathodic overpotentials ($|\eta_c| >> 0$; when totally irreversible reduction of oxygen ocures) Eq. 4.2.2 simplifies to

$$j = j_0 - \exp\left(-\frac{\alpha_\mathrm{c} nF\eta}{RT}\right) \qquad [4.2.5]$$

and

$$\alpha_c = -\frac{RT}{\eta_c nF} \ln\left|-\frac{j}{j_0}\right| \qquad [4.2.6]$$

It should be noted that the Butler-Volmer equation can be used for the studies of the electroreduction of oxygen under certain conditions, but this analysis gives no information about the microscopic details of the reaction. For that reason, various models have been developed [2,5,6,9,12–14,28,42,44–51]. According to these models the electroreduction of O_2 at porous cathode (and porous Pt as well) can take place only at the three-phase boundary (if $\eta \sim 0$) while both the TPB and the surface of $La_{1-x}Sr_xMnO_{3-\delta}$ can be active at the high overpotential values [12,48,49]. There are still considerable discrepancies in the reaction mechanism and rate determining steps for the O_2 reduction at various cathodes (LSMO, LSCFO etc.) [13,42,48–51], and therefore more information is needed for the detailed analysis of O_2 electroreduction at porous LSCO, PSCO and GSCO cathodes under study in this work.

4.3. Fitting of impedance data

Experimental impedance data were mainly analyzed using the equivalent circuits illustrated in Fig. 1, where R_{ex} is the total very high frequency series resistance of the system $R_{ex} \equiv Z_1(\omega \to \infty)$; CPE_1, R_1, CPE_2 and R_2 are the so-called high-frequency and low- frequency constant phase element and charge transfer resistance values, respectively; Z_W is Warburg-like diffusion impedance.

Usually constant phase element CPE is used in a model in place of a ideal capacitor to compensate the energetic and crystallographic non-homogeneity in the experimental system and can be expressed as

$$Z_{CPE} = \frac{1}{A(j\omega)^{\alpha}} \qquad [4.3.1]$$

where A is the CPE coefficient and α is the CPE fractional exponent. If $\alpha = 1$ then A is equal to the electrical double layer capacitance, if $\alpha = 0.5$ then $Z_{CPE} = Z_W$ and if $\alpha = 0$, then Z_{CPE} is equal to the resistance R [52–54].

Taking into account the masstransfer limited steps in complicated cathode matrix in equivalent circuit b in Fig. 1 the low-frequency constant phase element CPE_2 have been exchanged to the generalized finite Warburg element (GFW) for a short circuit terminus model expressed as

$$Z_{GFW} = \frac{R_D \tanh\left[\left(i\omega L^2 / D\right)^{\alpha_W}\right]}{\left(i\omega L^2 / D\right)^{\alpha_W}} \qquad [4.3.2]$$

where R_D is the limiting diffusion resistance, L is the effective diffusion layer thickness, D is the effective diffusion coefficient of a particle and α_w is a fractional exponent [52,54–61].

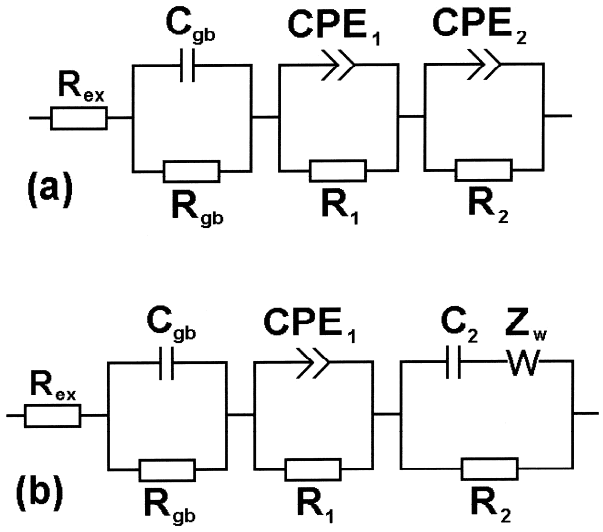

Figure 1. Equivalent circuits used for fitting the complex impedance plane plots. R_{ex} is the high-frequency series resistance ($R_{ex} \rightarrow Z'$ if $\omega \rightarrow \infty$); C_{gb} and R_{gb} are the grain boundary capacitance and resistance; CPE_1 and R_1 are the high-frequency constant phase element and resistance; CPE_2, R_2 and C_2 are the low-frequency constant phase element, resistance and capacitance, respectively; Z_W is the Warburg-like diffusion impedance.

There are two accurate ways to obtain an indication of how well the modeling function reproduces the experimental data set: the chi-square function (χ^2) and the weighted sum of the squares (Δ^2) give a main general indication about the quality of the fit and observing the parameter values and their relative error estimates (in %). [52,62].

5. EXPERIMENTAL

Commercially available powders of La_2O_3 (99.99%), Pr_6O_{11} (99.99%), Gd_2O_3 (99.9%), $SrCO_3$ (99.9 %) and Co_3O_4 (99.9 %) have been used for the synthesis of the $La_{0.6}Sr_{0.4}CoO_{3-\delta}$ (LSCO), $Pr_{0.6}Sr_{0.4}CoO_{3-\delta}$ (PSCO) and $Gd_{0.6}Sr_{0.4}CoO_{3-\delta}$ (GSCO) powders, using the conventional solid state reaction technique [2–6,57–61]. Powders with the stoichiometric compositions were ball-milled in a zirconia mill container with zirconia grinding balls in H_2O for 8 h and after drying calcined at 1473 K for 10 h to form a perovskite phase. The perovskite phase was crushed and ball-milled for 3 h using the same system. Thereafter the second temperature treatment cycle was made [57–61].

The $Ce_{0.8}Sm_{0.2}O_{2-\delta}$ (CSO) and $Ce_{0.8}Gd_{0.2}O_{2-\delta}$ (CGO) electrolytes were prepared from the corresponding oxides CeO_2 (99.9% Aldrich), Gd_2O_3 (99.9%) and Sm_2O_3 (99.8%), using conventional solid state reaction technique [2–6,57–61]. Powders with the stoichiometric compositions were ball-milled for 3 h and calcined at 1473 K in air for 10 h. The formed electrolyte materials were crushed and ball-milled in ethanol and thereafter two more temperature treatment cycles were made.

After adding an organic binder, the electrolyte powders were pressed into pellets with a diameter of 2 cm and thickness of 0.6 mm at the pressure p = 20 kN cm^{-2} for 0.5 min and thereafter sintered at 1473 K for 10 h. The cathode material synthesized was mixed with an appropriate amount of organic binder (ethyl cellulose) and solvent (turpentine oil) and screen-printed onto one side of the CGO electrolyte as a working electrode with the surface area S_{el} = 0.5 cm^2. The working electrodes were fired at 1323 K in air for 8 h. In some cases, the cathode material (LSCO) was activated by the Ag-nanoparticles, and for that the cathode material was impregnated with the $AgNO_3$ aqueous solution, followed by the decomposition and firing at 1073 K for 3 h. The mixed cathode materials was prepared by mixing 70 wt% LSCO (or LSCFO) with 30 wt% CGO powders before adding the organic binder and solvent. The following half-cells were prepared for electrochemical measurements:

Sys 1: $La_{0.6}Sr_{0.4}CoO_{3-\delta}$ | $Ce_{0.8}Gd_{0.2}O_{2-\delta}$
Sys 2: $Pr_{0.6}Sr_{0.4}CoO_{3-\delta}$ | $Ce_{0.8}Gd_{0.2}O_{2-\delta}$
Sys 3: $Gd_{0.6}Sr_{0.4}CoO_{3-\delta}$ | $Ce_{0.8}Gd_{0.2}O_{2-\delta}$
Sys 4: $La_{0.6}Sr_{0.4}CoO_{3-\delta}$ | $Ce_{0.85}Sm_{0.15}O_{2-\delta}$
Sys 5: $Pr_{0.6}Sr_{0.4}CoO_{3-\delta}$ | $Ce_{0.85}Sm_{0.15}O_{2-\delta}$
Sys 6: $Gd_{0.6}Sr_{0.4}CoO_{3-\delta}$ | $Ce_{0.85}Sm_{0.15}O_{2-\delta}$
Sys 7: 70wt% $La_{0.6}Sr_{0.4}CoO_{3-\delta}$ + 30wt% $Ce_{0.8}Gd_{0.2}O_{2-\delta}$ | $Ce_{0.8}Gd_{0.2}O_{2-\delta}$
Sys 8: 70wt% $La_{0.6}Sr_{0.4}Co_{0.8}Fe_{0.2}O_{3-\delta}$ + 30wt% $Ce_{0.8}Gd_{0.2}O_{2-\delta}$ | $Ce_{0.8}Gd_{0.2}O_{2-\delta}$
Sys 9: Ag + $La_{0.6}Sr_{0.4}CoO_{3-\delta}$ | $Ce_{0.8}Gd_{0.2}O_{2-\delta}$

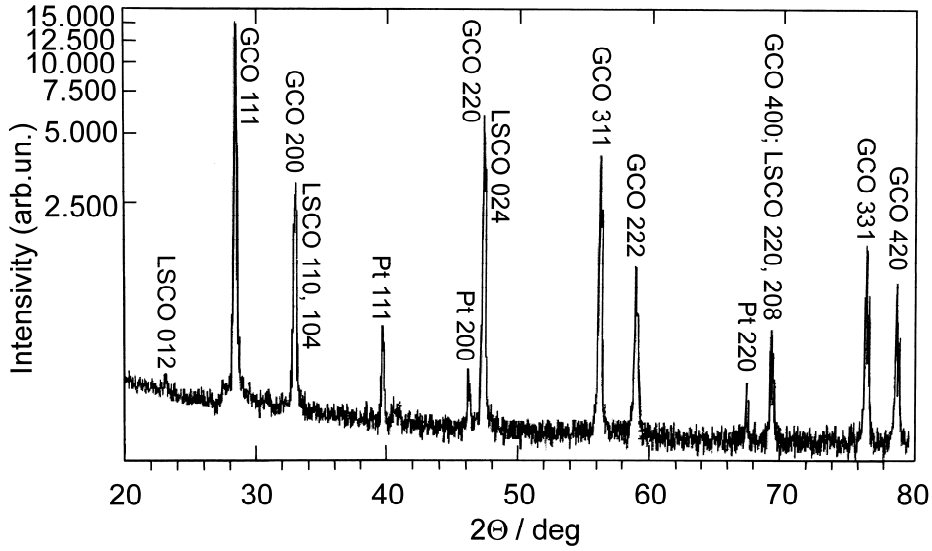

Figure 2. X-ray diffraction data for porous Pt | 70 wt% $La_{0.6}Sr_{0.4}CoO_{3-\delta}$ + 30 wt% $Ce_{0.8}Gd_{0.2}O_{2-\delta}$ | $Ce_{0.8}Gd_{0.2}O_{2-\delta}$ interface.

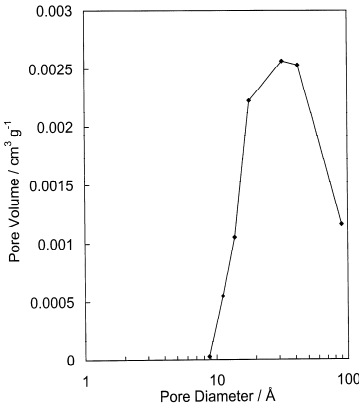

Figure 3. Incremental pore volume vs. pore diameter plot for the $La_{0.6}Sr_{0.4}CoO_{3-\delta}$ cathode (S_{BET} = 10.5 m g^{-1}).

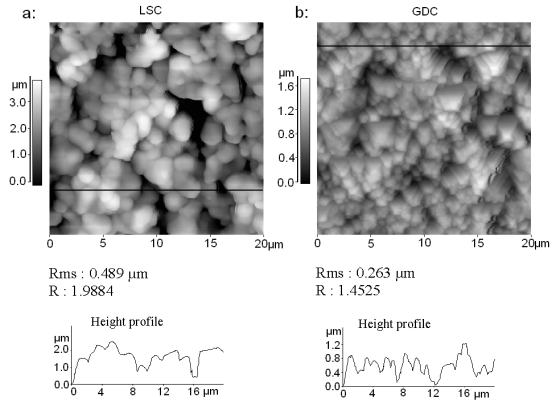

Figure 4. AFM images of microstructure of the $La_{0.6}Sr_{0.4}CoO_{3-\delta}$ cathode (a) and $Ce_{0.8}Gd_{0.2}O_{2-\delta}$ electrolyte (b), the corresponding height profiles and the values of the root mean square height (R_{ms}) and surface roughness $R = S_{AFM}/S_{geom}$.

The BET adsorption, X-ray diffraction and AFM methods have been used for the analysis of materials prepared. The X-ray diffraction measurements (Fig. 2) (Bragg-Brentano method) were made for all half-cells and usually ceria peaks, forming a very strong and intensive background, are seen as well as few cathode material peaks. Excluding the ceria peaks, we can see peaks, corresponding to the perovskite phase of cathode materials used and also peaks of Pt because a Pt

contact electrode was created and used to collect the current. No impurity peaks were observed for the cathode materials synthesized.

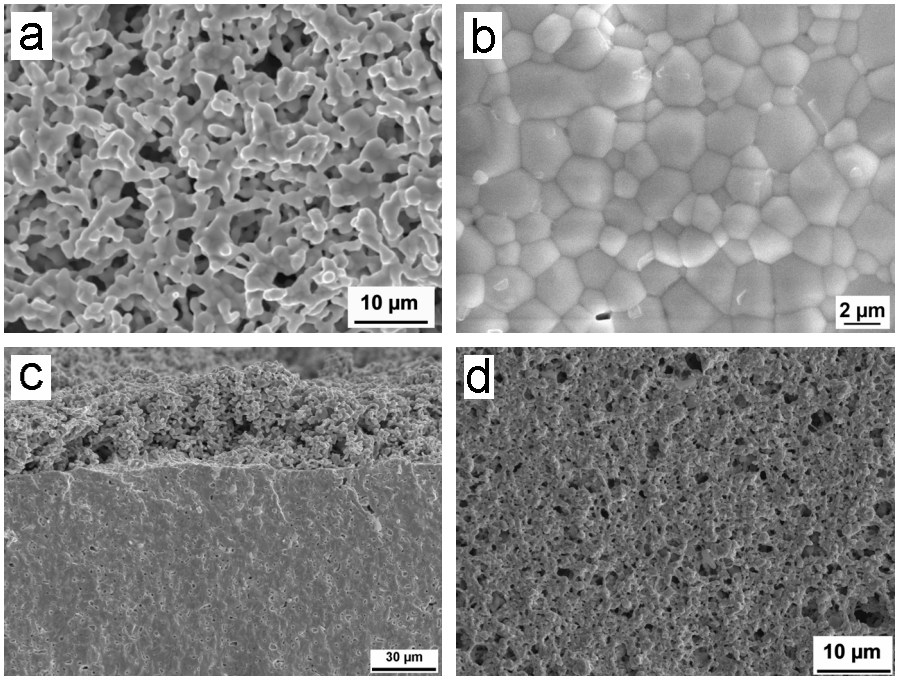

Figure 5. SEM images of the $La_{0.6}Sr_{0.4}CoO_{3-\delta}$ | $Ce_{0.8}Gd_{0.2}O_{2-\delta}$ half-cell: (a) cathode, (b) electrolyte, (c) cross-sectional view of the cathode and electrolyte and (d) Pt counter electrode.

Using the N_2 gas adsorption measurement method the specific surface area, pore size distribution, micropore volume and other gas phase characteristics have been obtained using Gemini 2375 system (Micrometrics Inc.). The specific surface area, obtained by the Brunauer, Emmett and Teller (BET) method, demonstrates comparatively high values for cathode materials (from 5 to 20 $m^2\ g^{-1}$). The nanopores with a medium pore size (15…18 Å) prevail inside cathode materials volume (Fig. 3). For the additional characterization of materials, the atomic force microscopy (AFM) studies were made (Fig. 4). It was found that there are no big pores inside the electrolyte. The surface structure of the solid electrolytes seems to be comparatively homogeneous and the very low values of $S_{BET} \sim 0$ have been obtained. The cathode materials (Fig. 4a) consists of aggregates consisting of spherical particles with a medium diameter of 1…2 μm and there are large pores ($d \sim 2…10$ μm) between these aggregates. It is reasonable because the cathode macro- and microstructure has to allow oxygen to diffuse to the reaction sites at the three-phase boundary (TPB) region. The surface profiles (Fig.4b), obtained using AFM method, indicate that the surface of the electrolyte is comparatively flat compared with

the cathode material surface. The same conclusion can be made taking into account the so-called AFM surface roughness factor values ($R_{AFM} = S_{AFM}/S_{geom}$) as well as the root mean square height values R_{ms} (S_{AFM} is the surface area of a material obtained by using AFM method and S_{geom} is the flat-gross section surface area).

The surface of cathode, electrolyte and Pt counter electrode have been investigated by SEM method. The very nice nanoporous cathode and Pt counter electrode have been prepared on the practically compact electrolyte as can be seen in Figure 5. The data for cathode | electrolyte interface show that there is very good contact between the cathode and electrolyte and there is no delamination between cathode and electrolyte layers. The electrolyte layer appears to be almost fully dense expect for some isolated pores, but no cross-layer pinholes or cracks are observed.

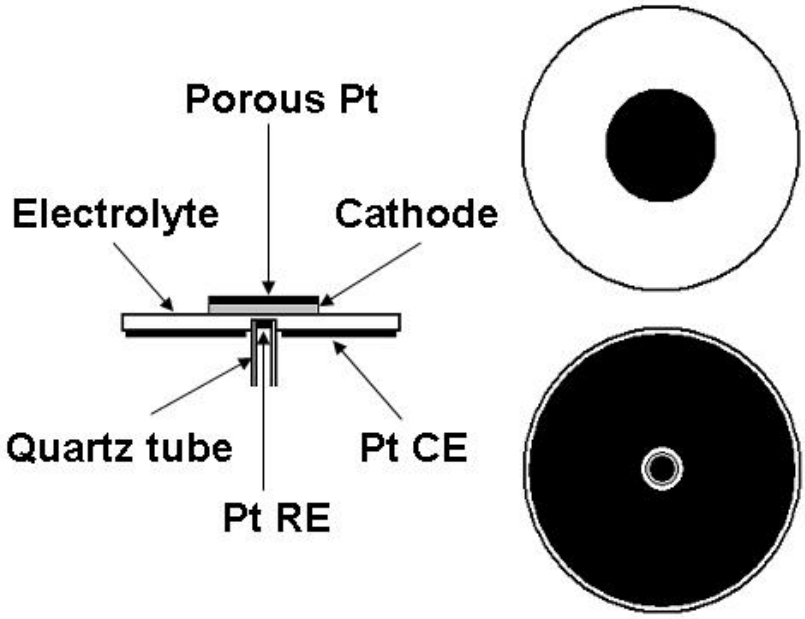

Figure 6. Experimental setup used for semicell studies.

A three-electrode assembly was used to study the electrochemical properties of the electrodes. The Pt counter and reference electrodes were prepared by screen-printing the Pt-paste (Engelhard) on the other side of the electrolyte, followed by sintering at 1223 K for 2 h. The areas of the Pt counter and Luggin-like reference electrodes were ~3 cm^2 and 0.04 cm^2, respectively (Fig. 6). The reference electrode (Pt | porous Pt | O_2) has been created into the hole prepared inside the solid electrolyte and the distance of the reference electrode to the working electrode was less than 10^{-2} cm. The lateral surface of the Pt-wire (i.e. the lateral surface of the reference electrode) has been isolated by Al_2O_3 capillary tube, introduced into the electrolyte pellet. The anode | electrolyte | cathode assembly was placed into designed reactor and cathode, reference

electrode and anode were exposed for air. Three Pt wires were connected to the working, counter and reference electrodes and led to the potentiostat/galvanostat (type 1287, Solartron), frequency response analyser (type 1260, Solartron). The ac frequency f was changed from 10 MHz to 0.01 Hz. The ac voltage amplitude was 5 mV. The impedance spectra were recorded at 10 points per decade.

6. RESULTS AND DISCUSSION

6.1. Nyquist plots

Comparison of impedance complex plane Z'',Z' (Nyquist) plots (where Z'' is imaginary and Z' is real part of impedance) for systems investigated (Fig. 7) indicates that the shape of impedance spectra noticeably depends on the chemical composition of the cathode studied i.e. on the A site position cation characteristics in the ABO_3 perovskite structure. The influence of the electrolyte composition on the shape of Z'',Z'-plots is noticeably smaller. The lowest very high frequency series resistance has been obtained for LSCO | CSO half cell (Sys 4) and the lowest low frequency polarisation resistance (R_p) values has been obtained for LSCO | CGO (Sys 1) and LSCO | CSO (Sys 4) half cells. For other half cells investigated R_p values increase in the order: PSCO | CSO (Sys 5) < GSCO | CSO (Sys 6) ≤ PSCO | CGO (Sys 2) ≤ GSCO | CGO (Sys 3) < 70wt% LSCO + 30wt% CGO | CGO (Sys 7) < 70wt% LSCFO + 30wt% CGO | CGO (Sys 8) < Ag + LSCO | CGO (Sys 9).

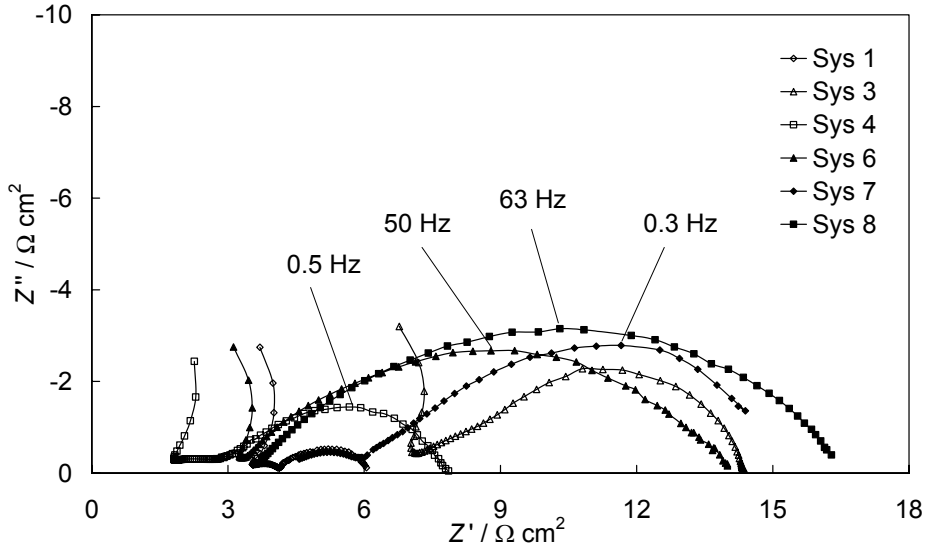

Figure 7. Z'',Z' (Nyquist) plots at T = 873 K for some systems investigated.

For systems with higher specific surface area (Sys 1, Sys 4, Sys 7 and Sys 8), the total polarisation resistance at f < 20kHz can be divided into two components: so-called medium-frequency polarisation resistance (R_{MF}; arc 1) and low-frequency polarisation resistance (R_{LF}, arc 2). Systematic analysis of the Nyquist plots shows that for the mixed cathodes (Sys 7 and Sys 8) the third very well developed semicircle has been established in the region of high frequencies (f > 20 kHz), corresponding to the mainly oxygen ion transfer process at the mixed cathode | electrolyte grain boundary. (R_{gb} and C_{gb} are the

oxygen ion resistance and capacitance at the grain boundary.) For all systems studied, the total polarisation resistance R_p decreases with increasing T and $|E|$.

The characteristic relation time τ_{max} (equal to $(2\pi f_{max})^{-1}$, where f_{max} is the frequency of the maximum in the Nyquist plot) obtained from the low frequency part of the Z'',Z'-plots depend noticeably on the chemical composition of cathode studied. The values of τ_{max} are nearly independent of the electrolyte composition if the same cathode material has been used. The noticeably lower values of τ_{max} have been obtained for Sys 8 and Sys 7 and τ_{max} decreases with rising the thermal fluctuation energy. Differently from the mixed cathodes (Sys 7 and Sys 8) the characteristic frequency for Sys1…Sys 6 is practically independent of the cathode potential applied.

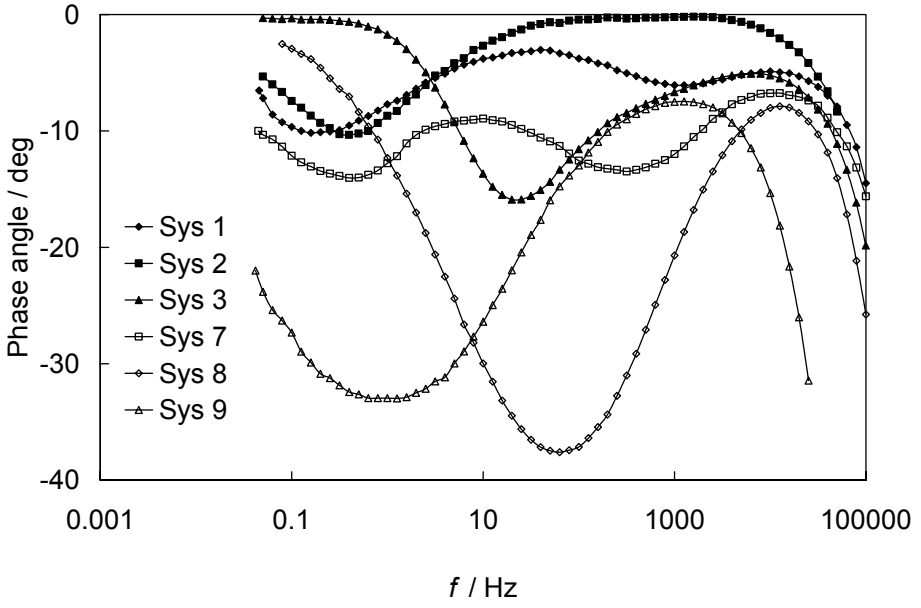

Figure 8. Phase angle vs. frequency plots at T = 773 K and ΔE = –0.1V.

The influence of the cathode material and T on the electrochemical characteristics and reaction mechanism, prevailing for O_2 reduction, is very well visible in the phase angle vs. log$f$ plots. The data for Sys 3, Sys 7 and Sys 8 and Sys 9 show that at $T \leq$ 773 K there prevails mixed kinetics behaviour (slow mass transfer (diffusion) and charge transfer steps) ($|\delta| \sim 30°$) (Fig. 8) (it should be noted that $\delta = -90^o$, $\delta = -45^o$ and $\delta = 0^o$ indicate adsorption, diffusion and charge transfer limited step mechanisms, respectively [52–54,58–61]). At higher negative potentials and higher temperature the systems tend toward purely charge transfer limited mechanism ($|\delta| \leq 5°$) (Fig. 9). However, the shape of δ,log$f$ plots shows that at $f \leq$ 20 kHz for systems with higher specific surface area (Sys 1, Sys 4 and Sys 7) there are two very well separable processes with different time constants. For other systems there seems to be only one (or two,

but not clearly separable) mainly diffusion-limited charge transfer process at $T \leq$ 773 K. The noticeable dependence of δ on ΔE indicates the very complicated mass transfer process (molecular diffusion, migration, surface diffusion of adsorbed ions, diffusion of oxygen ions inside mixed conducting cathode etc) of the charged oxygen species and O_2 in porous cathode for all systems studied (Fig. 10).

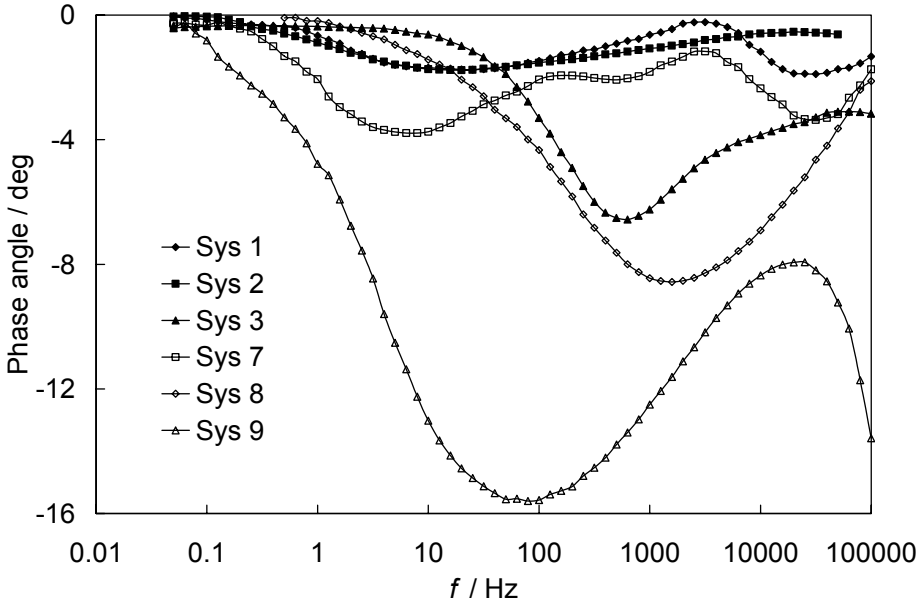

Figure 9. Phase angle vs. frequency plots at T = 973 K and ΔE = –0.1V.

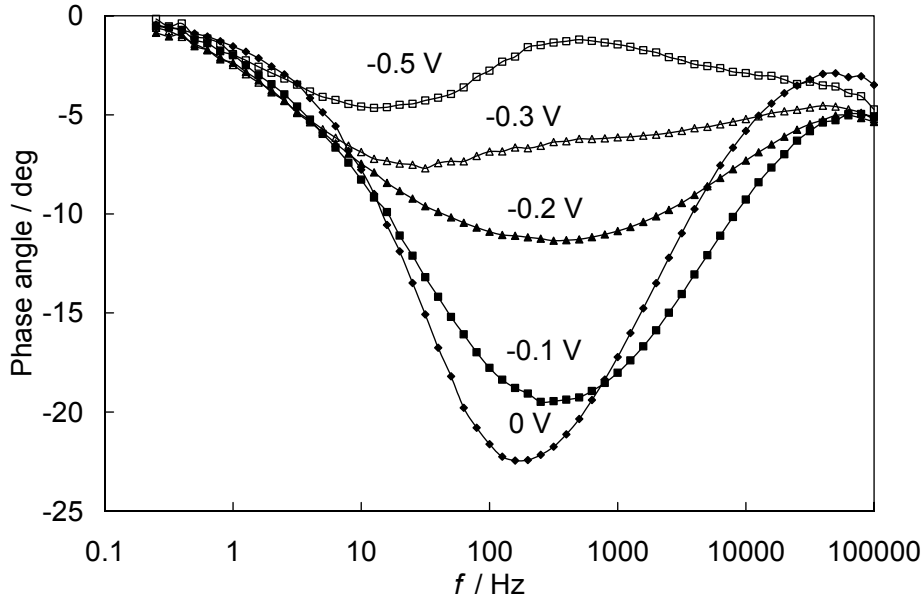

Figure 10. Phase angle vs. frequency plots for Sys 8 at T = 873 K in the case of various electrode polarizations ΔE (V) noted in figure.

6.2. Fitting of the complex impedance plane plots

The data in Nyquist plots, to a first approximation, can be simulated with the chi-square function $\chi^2 \leq 6\times10^{-4}$ and weighted sum of squares $\Delta^2 < 0.1$ by the equivalent circuit (a) presented in Fig. 1. The very high frequency series resistance R_{ex} is mainly determined by the electrolyte characteristics and according to the results of simulations, R_{ex} decreases with rising temperature and in the order of systems Sys 9 > Sys 3 > Sys 8 > Sys 7 > Sys 2 > Sys 1 > Sys 6 >Sys 5 > Sys 4 in the case of fixed temperature. Differently from the so-called mixed cathodes (Sys 7, Sys 8 and Sys 9), for Sys 1, Sys 2, Sys 3, Sys 4, Sys 5 and Sys 6 there is no very well separable semicircles in the region of high frequencies as the so-called grain boundary resistance R_{gb} has very low values. R_{gb} and C_{gb} are detectable for Sys 7 and Sys 8 only as there is noticeably higher interface area between porous mixed cathode and electrolyte and the values of R_{gb} decreases with increasing temperature and slightly with increasing the negative potential. The low values of R_{gb} indicate that the transfer of the charged O^{2-} ions at the grain boundary is relatively quick.

The medium as well as low frequency arcs can be fitted by the constant phase element CPE_1 and CPE_2 and charge transfer resistances R_1 and R_2 connected in parallel, respectively (Fig. 1a). The fractional exponent $\alpha_1 > 0.5$, very high C_1 and very low values of R_1 indicate that the so-called adsorption

like and "true" charge transfer limited processes are the rate-determining steps at $f > 10$ Hz and $T < 823$ K [52–54,58–61]. The values of C_1 (Fig. 11) increase with increasing T and ΔE, thus, the accumulation of partially reduced oxygen species into the cathode material takes place. At higher temperatures ($T > 873$ K) there are no very well separable semicircles in the region of medium frequencies and the equivalent circuits in Fig. 1 can be simplified within the frequency region from 0.01 to 10000 Hz and only the so-called low-frequency circuit, i.e. the low frequency process has mixed kinetics behavior.

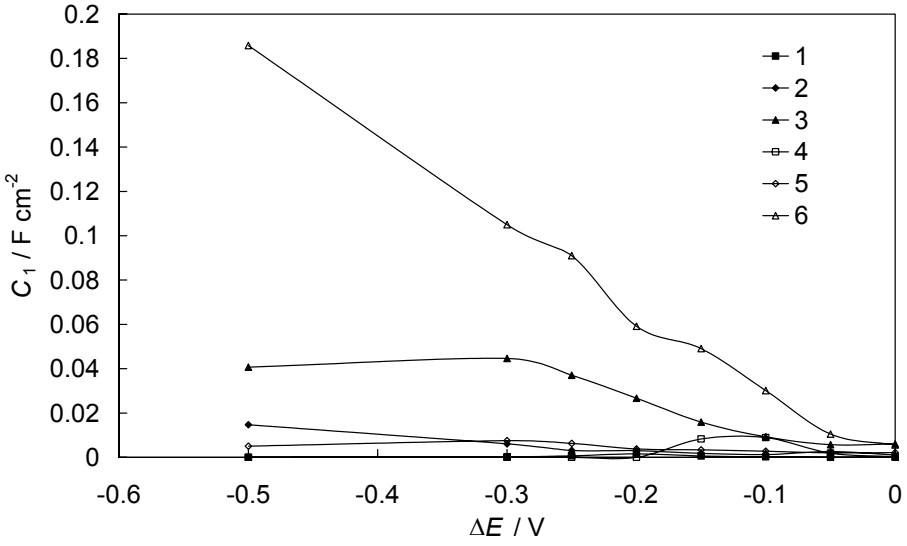

Figure 11. Medium frequency capacitance C_1 versus ΔE plots for Sys 4 (1; 4), Sys 6 (2; 5) and Sys 5 (3; 6) at $T = 773$ K (1–3) and $T = 873$ K (4–6).

The fractal exponent values $\alpha_2 \leq 0.5$ for CPE_2 (Fig. 1a) obtained for the low-frequency arc in the case of systems investigated indicate that CPE_2 behaves as a Warburg- type diffusion impedance. Thus, at low frequencies, the CPE_2 can be exchanged to the generalized finite length Warburg element (GFW) for a short circuit terminus model (Fig. 1b) [52–54,58–61]. The very small chi-square function values $\chi^2 < 2\times10^{-4}$ and weighted sum of squares $\Delta^2 < 0.03$ have been established [58–61]. The relative residuals obtained for this circuit are very low and have a random distribution in the whole frequency region studied. Therefore it seems that the low-frequency arc at $T \leq 873$ K characterizes the kinetically mixed, charge transfer and mass transfer (diffusion-like) limited adsorption processes ($|\delta| < 15°$), taking into account the very high C_2 values obtained. The values of $\alpha_W \leq 0.5$ indicate that there are deviations from the classical semi-infinitive diffusion model toward the generalized finite length Warburg diffusion model [56–61], i.e. toward the anomalous diffusion model with the adsorption boundary condition [63–65]. The diffusion resistance R_D (Fig. 12) and the low-frequency charge transfer resistance R_2 (Fig. 13) decrease

with increasing temperature and $|E|$ if $\Delta E \leq -0.2$ V and in the order of systems Sys 9 > Sys 7 ≥ Sys 8 > Sys 3 ≥ Sys 2 > Sys 6 ≥ Sys 5 ≥ Sys 1 ≥ Sys 4. The dependence of R_D on ΔE, indicates the very complicated mass transfer process as the resistance of the semi-infinite Fick-like diffusion process has to be independent of ΔE. The surface diffusion, Knudsen-like and finite-length diffusion as well as migration of charged oxygen species are possible. At fixed temperature and $\Delta E > -0.2$ V the values of R_D are noticeably higher than R_2, indicating the mainly mass transfer limited reaction mechanism. The noticeable dependence of so called frequency parameter T_W ($T_W = L^2D^{-1}$) on ΔE at $\Delta E < -0.2$ V in the case of fixed T can be explained by reduction of the effective reaction layer thickness with increasing the cathodic potential and temperature if we assume that diffusion (masstransfer in reality) coefficient D is independent of ΔE. At higher ΔE the additional transport mechanisms of oxygen ions (surface diffusion/migration) are possible. At higher temperature (i.e. under conditions of the very effective thermal activation) T_W is independent of ΔE. The low-frequency capacitance C_2 (i.e. adsorption, absorption capacitance or pseudocapacitance of the reduction process) decreases with rising temperature and increases in the reverse order as R_D (Fig. 14). The increase of C_2 with $|\Delta E|$ at lower temperature (except Sys 9) can be explained by accumulation (adsorption or absorption) of the negatively charged oxygen anions into the porous cathode material as well as by increase of the pseudocapacitance of the oxygen reduction reaction at moderate temperature and ΔE.

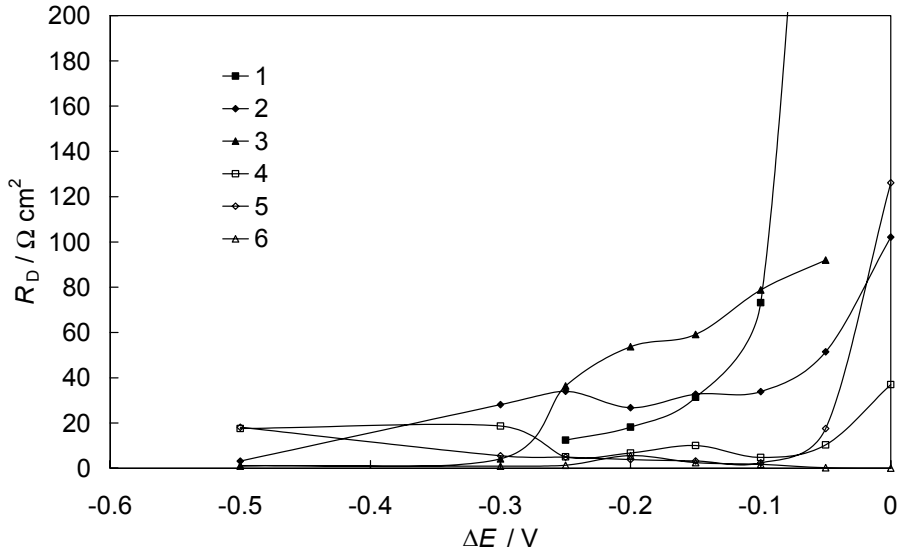

Figure 12. Diffusion resistance R_D versus electrode potential dependences for Sys 4 (1; 4), Sys 6 (2; 5) and Sys 5 (3; 6) at T = 773 K (1–3) and T = 873 K(4–6).

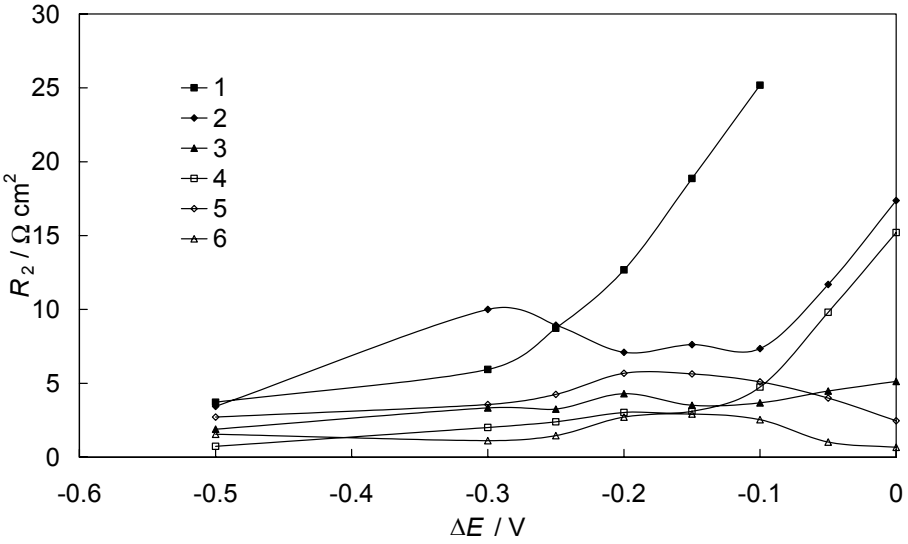

Figure 13. Low-frequency charge transfer resistance R_2 versus electrode potential dependences for Sys 4 (1; 4), Sys 6 (2; 5) and Sys 5 (3; 6) at T = 773 K (1–3) and T = 873 K(4–6).

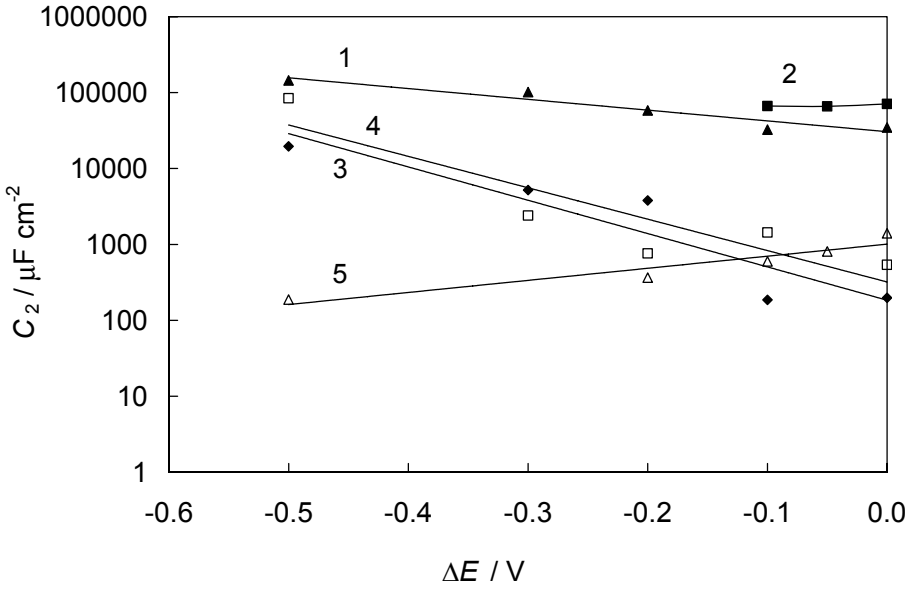

Figure 14. Capacitance C_2 vs. ΔE-plots at T = 873 K for Sys 1 (1), Sys 4 (2), Sys 7 (3), Sys 8 (4) and Sys 9 (5)

6.3. Activation energy, current relaxation plots and transfer coefficient

The capacitive parts of the impedance spectra at $f \leq 20$ kHz were used to determine the polarization resistance (R_p) from the difference between the intercepts of the very low and high frequency parts of the spectra with the Z'-axis of Nyquist plots. Comparison of the data shows that the total polarization resistance increases in the order Sys 4 < Sys 1 < Sys 5 < Sys 6 ≤ Sys 2 ≤ Sys 3 < Sys 8 < Sys 7 < Sys 9. Thus, noticeably higher R_p values have been obtained for Sys 9, which is caused by the very high mass transfer resistance inside the nanopores [56–61]. The nonlinear shape of Arrhenius plots indicates the change in the nature of the limiting process with increasing temperature. The value of activation energy E_{act} (Fig 15) for Sys 3, Sys 5, Sys 6 and Sys 7, obtained from Z',Z'-plots, is in a reasonable agreement with the value of A_D, obtained from the diffusion resistance R_D vs. temperature plots. Thus, the arc 2 for these systems at lower T characterizes mainly the mass transfer (i.e. diffusion-like) limited process of the electrochemically active oxygen pieces.

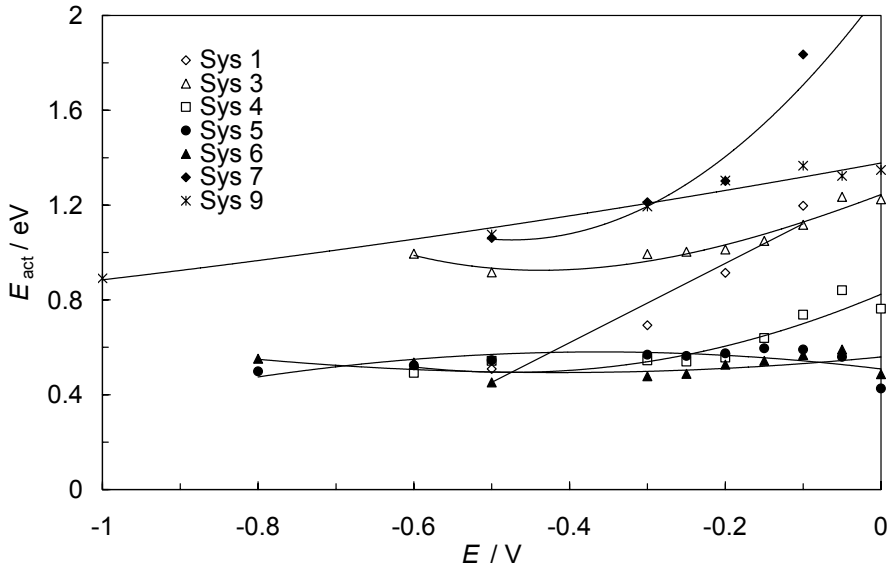

Figure 15. Activation energy vs. electrode potential plots for half-cells, noted in figure.

Chronoamperometry curves obtained indicate that the shape of the j_c,t-curves depends on T, ΔE, as well as on the electrolyte and cathode compositions (Fig. 16). At small times ($t < 2.0$ s) $|j_c|$ increases with time. The stable $|j_c|$ values have been established at $T \leq 773$ K in the case of $t > 5.0$ s, but at $T \geq 973$ K at very short charging times $t < 1$ s. At lower temperatures ($T \leq 773$ K) the cathodic current density (i.e. the rate of cathodic reaction) is noticeably higher for Sys 4 than for other systems (j_c increases in the order Sys 9 < Sys 8 < Sys 7 < Sys 3 <

Sys 2 < Sys 1 ≤ Sys 6 < Sys 5 ≤ Sys 4) [56–61]. The increase in the cathode current density with time can be explained by extending the active reaction zone from the open surface area to the porous surface of mixed conducting cathode. The increase in concentration of the "charged oxygen" pieces with increasing the negative cathode potential will improve the catalytic activity of the cathode and the decrease in the values of E_{act} is in a good agreement with experimental results obtained. However, the fitting data of the Z',Z'-plots show that the oxygen reduction in Sys 9, Sys 7, Sys 8, Sys 6 and Sys 3 is mainly limited by the mixed kinetics, i.e. charge transfer and diffusion-like steps, in the porous cathode material when the higher cathodic potential is applied to the interface.

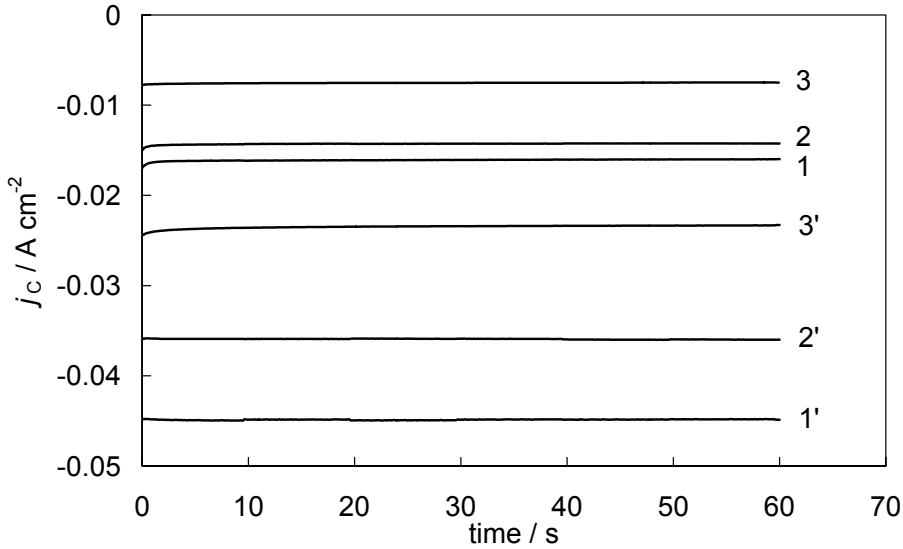

Figure 16. Chronoamperometry data for $La_{0.6}Sr_{0.4}CoO_{3-\delta}$ (1; 1'), $Pr_{0.6}Sr_{0.4}CoO_{3-\delta}$ (2; 2') and $Gd_{0.6}Sr_{0.4}CoO_{3-\delta}$ (3; 3') cathodes on the $Ce_{0.8}Gd_{0.2}O_{2-\delta}$ electrolyte at T = 873 K (1–3) and T = 973 K (1'–3').

The Tafel-like overpotential η,lnj_c-curves have been calculated from the j_c,t-curves at t > 10 s when the stable values of j_c have been established at fixed ΔE and T. (ΔE values have been corrected by the ohmic potential drop $\Delta U = IR$ to obtain η). According to the calculations, the values of transfer coefficient, α_c, higher than 0.5 for Sys 1, Sys 2, Sys 3, Sys 5, Sys 6, Sys 7 and Sys 8 indicate the mixed kinetic mechanism, i.e. slow O_{ads}^- or O_{ads} diffusion, in addition to slow electron transfer seems to be the rate-determining step [56–61]. The values of α_c for the systems studied increase slightly with rising temperature. The exchange current density (j_0), obtained from the Tafel plots (Fig. 17), increases with temperature and in the order of systems Sys 9 < Sys 7 < Sys 8 < Sys 3 < Sys 6 ≤ Sys 4< Sys 5 ≤ Sys 1 < Sys 2.

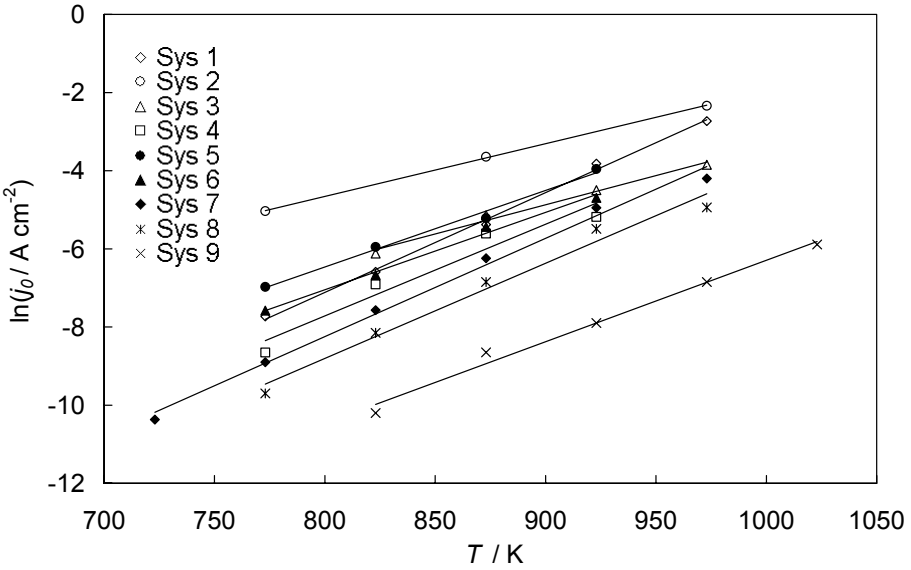

Figure 17. The exchange current density versus temperature plots for half-cells investigated (noted in figure).

6.4. Influence of operation time on the electrochemical characteristics of half-cells

The long-term stability has been tested at $T = 973$ K and $\Delta E = -0.3$ V for Sys 1 (4600 hours), Sys 2 (1200 hours), Sys 4 (1500 hours), Sys 7 (3000 hours) and Sys 9 (4600 hours). It should be noted that during the operation period the thermocycle has been made after every 100 working hours. According to the experimental results at higher temperature ($T \geq 873$ K), the shape of the Z'',Z'-plots is practically independent of operation time. At short working time ($t <$ 200 h) the small decrease in R_p has been observed (Fig. 18), but at $t > 300$ h the stabilization of the electrochemical parameters has been established. At lower temperature ($T \leq 773$ K), the small decrease of low-frequency polarization resistance (R_p) has been established at operation time from 200 to 1000 hours.

The values of high-frequency series resistance $Z'(\omega \to \infty) = R_{ex}$ for all systems studied do not depend noticeably on the operation time (Fig. 19). Thus, there is no delamination of the cathode layer from the electrolyte surface for system studied. For Sys 7 there is a noticeable increase in R_p at longer operation times ($t > 3000$ h), which is caused by the increase of the charge transfer resistance and by the degradation of the composite cathode. The time stability of R_p is somewhat lower for Sys 9, where the restructuring of the Ag clusters takes probably place on the LSCO surface during the long-lasting O_2 reduction process.

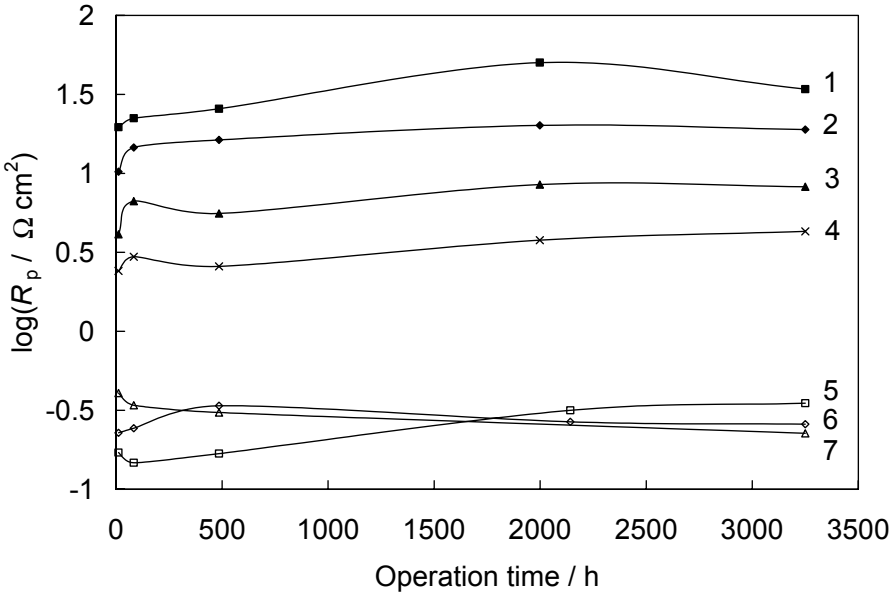

Figure 18. Dependences of log R_p on operation time for Sys 1. The curves 1–4 are obtained at T = 773 K and curves 5–7 at 973 K at the electrode polarizations ΔE (V): –0.1 (1; 5), –0.2 (2; 6), –0.3 (3; 7), and –0.5 (4).

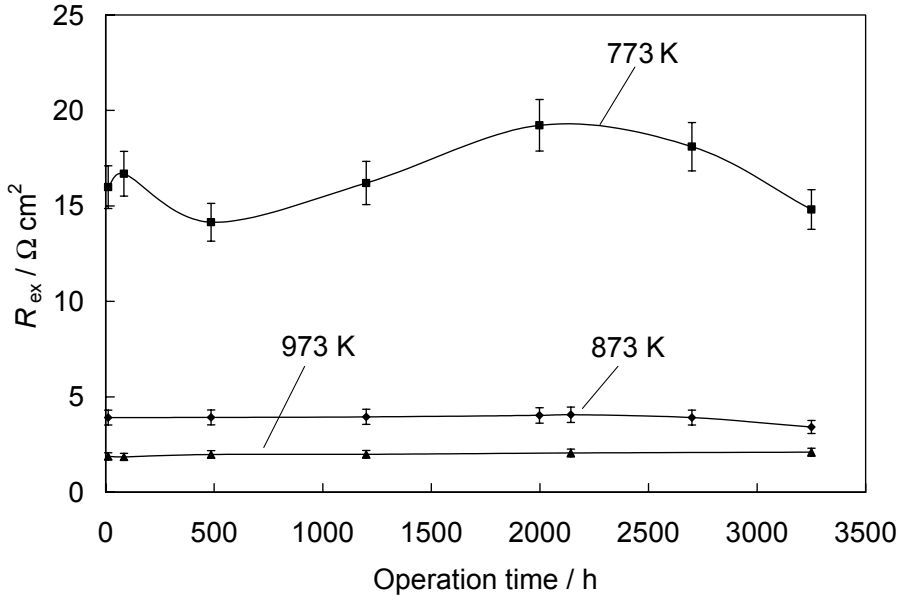

Figure 19. Dependences of $R_{ex} = Z'(\omega \rightarrow \infty)$ on operation time for Sys 1 at temperatures, noted in figure.

The results of fitting the Z'',Z'-plots show that the diffusion resistance R_D, low-frequency charge transfer resistance R_2, adsorption capacitance C_2 and fractional exponent of diffusion impedance α_W are practically independent of operation time if $T \geq 823$ K. At $T \leq 773$ K, there is small increase of R_D and α_W for Sys 1, Sys 2 and Sys 4 at $t > 1000$ hours, but more pronounced increase in R_D for Sys 7, and Sys 9 has been established. The parallel charge transfer resistance R_2 is practically independent of operation time if $T \geq 823$ K, and only at $T \leq 773$ K, R_2 very weakly increases with time.

At $|\Delta E| > 0.1$ V, the activation energy only very slightly changes with operation time $1000 < t < 3000$ h. The current density j_c decreases somewhat with operation time at lower polarizations, but this dependence is very small at $|\Delta E| \geq 0.2$ V. The transfer coefficient α_c for oxygen reduction is practically independent of the operation time. So, there are no changes in the reaction mechanism of oxygen reduction during long operation times.

7. SUMMARY

Electrochemical characteristics of various half-cells, based on samaria and gadolinia doped ceria electrolytes and $La_{0.6}Sr_{0.4}CoO_{3-\delta}$, $Pr_{0.6}Sr_{0.4}CoO_{3-\delta}$ and $Gd_{0.6}Sr_{0.4}CoO_{3-\delta}$ cathodes as well as so called mixed cathodes 70 wt% $La_{0.6}Sr_{0.4}CoO_{3-\delta}$ + 30 wt% $Ce_{0.8}Gd_{0.2}O_{2-\delta}$, 70 wt% $La_{0.6}Sr_{0.4}Co_{0.8}Fe_{0.2}O_{3-\delta}$ + 30 wt% $Ce_{0.8}Gd_{0.2}O_{2-\delta}$ and Ag + $La_{0.6}Sr_{0.4}CoO_{3-\delta}$ have been obtained by electrochemical impedance, cyclic voltammetry and chronoamperometry methods. X-ray diffraction, scanning electron microscopy, atomic force microscopy and gas adsorption measurement methods have been used for comparative analysis of physical properties of cathodes and electrolytes under study.

Detailed analysis of the complex impedance (Z'',Z') plots shows that the total polarization resistance increases with the rise of atomic mass of the cation in the A-site position of perovskite – like structure, as well with adding electrolyte or metallic Ag into the cathode material structure. The phase angle versus ac frequency plots indicate that at $T \leq 773$ K the mixed kinetics behavior prevails for most half-cells studied (slow mass transfer and charge transfer limiting steps). At higher negative potentials and temperatures the systems tend toward purely charge transfer limited oxygen electroreduction mechanism ($\delta \geq -5°$). However, the noticeable dependence of δ on ΔE indicates the very complicated mass transfer process of the charged oxygen species in porous cathode.

The various equivalent circuits have been used for fitting the Nyquist (Z'',Z'–) plots. A better fit has been established using a model corresponding to the equivalent circuit where the charge transfer process at grain boundaries (at high frequencies) and the medium and low frequency O_2 electroreduction process at the open cathode surface and inside the porous cathode material have been taken account. The low-frequency series resistance and diffusion resistance values increase in the order $La_{0.6}Sr_{0.4}CoO_{3-\delta}$ < $Pr_{0.6}Sr_{0.4}CoO_{3-\delta}$ < $Gd_{0.6}Sr_{0.4}CoO_{3-\delta}$ < mixed cathodes, while Ag + $La_{0.6}Sr_{0.4}CoO_{3-\delta}$ cathode demonstrates the highest low-frequency series resistance and diffusion resistance values.

The kinetically mixed process (slow mass transport and electron transfer stages) seems to take place for all systems studied. The values of activation energy, decreasing with the increasingly negative cathode potential, and the transfer coefficient $\alpha_c > 0.5$ indicate that in addition to the slow electron transfer process (reduction of oxygen) the mass transfer process of electrochemically active species in solid cathode material or at the internal porous cathode surface can probably be the rate – determining steps in agreement with the fitting results of the Nyquist plots.

The operation time stability test results show that electrochemical characteristics for half-cells have a good stability during long operation times (thousands of hours). More pronounced dependence of the electrochemical

characteristics on operation time is possible for the Ag + $La_{0.6}Sr_{0.4}CoO_{3-\delta}$ | $Ce_{0.8}Gd_{0.2}O_{2-\delta}$ half-cell, where the restructuring of the Ag clusters takes probably place on the LSCO surface during the long-duration O_2 electro-reduction process.

8. REFERENCES

[1] N.P. Brandon, S. Skinner, B.C.H. Steele, Annu. Rev. Mater. Res. 33 (2003) 183.
[2] S. C. Singhal, Solid State Ionics 135 (2000) 305.
[3] Weber, E. Ivers-Tiffée, J. Power Sources 127, (2004) 273.
[4] V. Dusastre, A. Kilner, Solid State Ionics 126 (1999) 163.
[5] S. P. Jiang, Solid State Ionics 146 (2002) 1.
[6] M. Mogensen, N. M. Sammes, G. A. Tompsett, Solid State Ionics 129, (2000) 63.
[7] S.B. Adler, Solid State Ionics 111 (1998) 125.
[8] Reiss, D. Braunshtein, D.S. Tannhauser, J. Amer. Ceram. Soc. 64 (1981) 479.
[9] S. B. Adler, J. A. Lane, B. C. H. Steele, J. Electrochem. Soc. 143 (1996) 3354.
[10] G. Ch. Kostogloudis, Ch. Ftikos, Solid State Ionics 126 (1999) 143.
[11] Y. Teraoka, T. Nobunaga, K. Okamoto, M. Miura, N. Yamazoe, Solid State Ionics 48 (1991) 207.
[12] S. Wang, X. Lu, M. Liu, J. Solid State Electrochem. 6 (2002) 384.
[13] M. Godickemeier, K. Sasaki, L. J. Gauckler, I. Riess, J. Electrochem. Soc. 144 (1997) 1635.
[14] S. Wang, T. Kato, S. Nagata, T. Honda, T. Kaneko, N. Iwashita, M. Dokiya, J. Electrochem. Soc. 149 (2002) A 927.
[15] E. Siebert, A. Hammouche, M. Kleitz, Electrochim. Acta 40 (1995) 1741.
[16] Ringuede, J. Fouletier, Solid State Ionics 139 (2001) 167.
[17] M. Kleitz, F. Petitbon, Solid State Ionics 92 (1996) 65.
[18] Ringuedé, J. Guindet, Ionics 3 (1997) 256.
[19] N. Imanishi, T. Matsumura, Y. Sumina, K. Yoshimura, A. Hirano, Y. Takeda, D. Mori, R. Kanno, Solid State Ionics 174 (2004) 245.
[20] S.P. Jiang, Y.J. Leng, S.H. Chan, K.A. Kohr, Electrochem. and Solid State Letters 6 (2003) A67–70.
[21] E.P. Murray, T. Tsai, S.A. Barnett, Solid State Ionics 110 (1998) 235.
[22] E.P. Murray, S.A. Barnett, Solid State Ionics 143 (2001) 265.
[23] T. Horita, K. Yamaji, N. Sakai, H. Yokokawa, T. Kawada, T. Kato, Solid State Ionics 127 (2000) 55.
[24] K. Yasumoto, M. Shiono, H. Tagawa, M. Dokiya, K. Hirano, J. Mizusaki, J. Electrochem. Soc. 149 (2002) A531.
[25] L. Tsai, S.A. Barnett, Solid State Ionics 93 (1997) 207.
[26] M.J.L. Ostergard, C. Clausen, C. Bagger, M. Morgensen, Electrochim. Acta 40 (1995) 1971.
[27] V.A.C. Haanappel, J. Mertens, D. Rutenbeck, C. Tropartz, W. Herzhof, D. Sebold, F. Tietz, J. Power Sources 141 (2005) 216.
[28] B. C. H. Steele, Solid State Ionics 129 (2000) 95.
[29] C. Chervin, R.S. Glass, S.M. Kauzlarich, Solid State Ionics 176 (2005) 17.
[30] R.A. De Souza, J.A. Kilner, Solid State Ionics 106 (1998) 175.
[31] T. Kawada, K. Masuda, J. Suzuki, A. Kaimai, K. Kawamura, Y. Nigara, J. Mizuaki, H. Yugami, H. Arashi, N. Sakai, H. Yokokawa, Solid State Ionics 121 (1999) 271.
[32] H.U. Anderson, in F.W. Poulsen, J.J. Bentzen, T. Jacobsen, E. Skou, M.J.L. Ostergard, Eds), Proc. 14th Risø Int. Symp. on Mat. Sci: High Temperature

Electrochemical Behaviour of Fast Ion and Mixed Conductors, Risø Nat. Lab. Roskilde, 1993, p. 1.
[33] H. Fukunaga, M. Koyama, N. Takahashi, C. Klen, K. Yamada, Solid State Ionics 132 (2000) 279.
[34] D. Waller, J.A. Lane, J.A. Kilner, R. J. Chater, P.S. Manning, B.C.H. Steele, in B. Thorstensen (Ed.), Proc. 2nd Eur. SOFC Forum, Vol. 2, 1996, p. 737.
[35] K. Masuda, A. Kaimai, K. Kawamura, Y. Nigara, T. Kawada, J. Mizusaki, H. Yugami, H. Arashi, in U. Stimming (Ed.), Proc. 5th Int Symp. SOFC, Electrochem. Proc. Ser. PV 97–18, Pennington, NY, 1997, p. 473.
[36] S.W. Matin, Solid State Ionics 51 (1992) 19.
[37] E.P. Murry, M.J. Sever, S.A. Barnett, Solid State Ionics 198 (2002) 27.
[38] J. van Herle, D. Senevirante, A.J. McEvoy, J. Europ. Ceram. Soc. 19 (1999) 843.
[39] C.E. Baumgartner, R.H. Arendt, C.D. Iacovangelo, B.R. Karas, J. Electrochem. Soc. 131 (1984) 2217.
[40] H. Ullmann, N. Trofimenko, F. Tietz, D. Stöver, A. Ahmad-Khanlou, Solid State Ionics 138 (2000) 79.
[41] S.H. Chan, X.J. Chen, K.A. Khor, J. Electrochem. Soc. 151 (2004) A154.
[42] G.O. Yamamoto, Electrochimica Acta 45, (2000) 2423.
[43] J. O'M. Bockris, A. K. N. Reddy, Modern Electrochemisty, Vol. 2, Plenum Press, New York, (1998).
[44] S. P. S. Badwal, Solid State Ionics 143, (2001) 39.
[45] N.Q. Minh, J. Am. Ceram. Soc. 76, (1993) 563.
[46] T. Horita, K. Yamaji, N. Sakai, H. Yokokawa, A. Weber, E. Ivers-Tiffee, Solid State Ionics 138, (2000) 143.
[47] T. Ishihara, S. Fukui, H. Nishiguchi, Y. Takita, J. Electrochem. Soc. 149, (2002) A 823.
[48] D. Y. Wang, A. S. Nowick, J. Electrochem. Soc. 126, (1979) 1155.
[49] Y. Jiang, S. Wang, Y. Zang, J. Yan, W. Li, Solid State Ionics 110, (1998) 111.
[50] K. Wippermann, in Materials and Mechanism, K. Nisancioglu, Editor, p. 31, Proceedings of TEA Workshop, Wadahl, Norway (1999).
[51] F. H. van Heuveln, H. H. M. Bouwmeester, J. Electrochem. Soc. 144, (1997) 134.
[52] J.R. MacDonald, W.B. Johnson, in J.R. MacDonald (Ed.), Impedance Spectroscopy: Emphasizing Solid Materials and Systems, Wiley, New York, 1987.
[53] M. Sluyters-Rehbach, J. Sluyters, in A. Bard (ed.) Electroanalytical Chemistry, Vol. 4, Macel Dekker, New York, 1970, p. 76.
[54] Lasia, in B.E. Conway, J. O'M. Bockris, R.E. White (Eds.), Modern Aspects of Electrochemistry, Vol 32, Kluwer Academic / Plenum Publishers, New York, 1999, p 143.
[55] E. Lust, G. Nurk, P. Moller, I. Kivi, S. Kallip, A. Jänes, V. Sammelselg, H. Mändar, Proc. of the Internat. Symp. on Solid Oxide Fuel Cells, Paris, 2003 p. 1176.
[56] G. Nurk, S. Kallip, I. Kivi, P. Möller, E. Lust, Proc. of 6th European Fuel Cell Forum, Lutzern, 2004, p. 887.
[57] E. Lust, G. Nurk, S. Kallip, I. Kivi, P. Möller, P. Nigu, K. Lust, Proc. of 6th European Fuel Cell Forum, Lutzern, 2004, p. 1271.
[58] E. Lust, G. Nurk, P. Möller, I. Kivi, S. Kallip. 26th Risø International Symposium on Materials Science, Risø, 2005, p. 279.

[59] E. Lust, G. Nurk, S. Kallip, I. Kivi, P. Möller. Journal of Solid State Electrochemistry, 9 (2005) 674.
[60] E. Lust, P. Möller, I. Kivi, G. Nurk, S. Kallip. Journal of Solid State Electrochemistry, 9 (2005) 882.
[61] E. Lust, P. Möller, I. Kivi, G. Nurk, S. Kallip, P. Nigu, K. Lust. Journal of the Electrochemical Society, 152 (2005) A2306.
[62] ZPLOT for Windows (Version 2.2) fitting program, Scribner Inc., Southern Pines, North Carolina.
[63] T. Jakobsen, K. West, Electrohim. Acta, 40 (1995) 233
[64] A. Compte, Phys. Rew. 53 (1996) 4191
[65] J. Bisquert, A. Compte, J. Electoanal. Chem. 499 (2001) 112

9. SUMMARY IN ESTONIAN

Mõningate tahkefaasireaktsiooni meetodil sünteesitud keskmistel temperatuuridel töötava tahkeoksiidkütuselemendi katoodimaterjalide elektrokeemiline karakteriseerimine

Käesolevas töös uuriti perovskiitseid katoodimaterjalide $La_{0.6}Sr_{0.4}CoO_{3-\delta}$, $Pr_{0.6}Sr_{0.4}CoO_{3-\delta}$ ja $Gd_{0.6}Sr_{0.4}CoO_{3-\delta}$ ning niinimetatud segukatoodide 70% $La_{0.6}Sr_{0.4}CoO_{3-\delta}$ + 30% $Ce_{0.8}Gd_{0.2}O_{2-\delta}$, 70% $La_{0.6}Sr_{0.4}Co_{0.8}Fe_{0.2}O_{3-\delta}$ + 30% $Ce_{0.8}Gd_{0.2}O_{2-\delta}$ ja Ag + $La_{0.6}Sr_{0.4}CoO_{3-\delta}$ elektrokeemilist käitumist samaariumi ja gadoliiniumiga dopeeritud tseeriumoksiid elektrolüütidel impedantsspektroskoopia, kronoamperomeetria ja tsüklilise voltamperomeetria meetoditega. Sünteesitud katoodi- ja elektrolüütimaterjalide füüsikaliste omaduste uurimiseks kasutati röntgenstruktuuranalüüsi, elektronmikroskoopia, aatomjõumikroskoopia ja gaasi adsorbtsiooni (Brunauer – Emmett – Teller) meetodeid ning võrreldi saadud parameetreid (makro- ja mikropoorsus, kristallilisuse aste, eripind, pooride keskmistatud jaotus jne) elektrokeemiliste andmetega.

Impedantsspektroskoopia andmete analüüsimisel saadud tulemustest selgub, et perovskiidi A-positsioonis oleva elemendi aatommassi kasvades polarisatsiooniline takistus kasvab, samuti kasvab polarisatsiooniline takistus lisades katoodi struktuuri elektrolüüdimaterjali või katoodi pinnale metallilise hõbeda osakesi. Faasinurga sagedusest sõltuvustest selgub, et madalamatel temperatuuridel ($T \leq 773$ K) on valdavalt tegemist segakineetiliste protsessidega (limiteerivaks on nii laenguülekande kui ka massiülekande protsessid), kuid kõrgematel temperatuuridel ja elektroodi polarisatsioonidel viitavad faasinurga suhteliselt väikesed negatiivsed väärtused ($\delta \geq -5°$) põhiliselt laenguülekande poolt limiteeritud protsessile. Faasinurga väärtuste oluline sõltuvus elektroodi polarisatsioonist madalamatel temperatuuridel viitab komplitseeritud laetud hapniku osakeste massiülekandeprotsessile poorses katoodis.

Nyquisti (Z',Z'') sõltuvuste modelleerimiseks kasutati kahte erinevat ekvivalentskeemi. Parem kokkulangevus saadi ekvivalentskeemiga, kus kasutatakse mudelit, mis võtab arvesse laenguülekande protsessi osakeste piirpindadel (kõrgematel sagedustel) ja hapniku elektroredutseerumisprotsessi katoodi piirpinnal ning poorse katoodimatejali sisemuses, mis leiab aset madalamatel ja keskmistel sagedustel. Madalsageduslik järjestikune takistus ja diffusiooniline takistus kasvavad katoodimaterjalide järjestuses $La_{0.6}Sr_{0.4}CoO_{3-\delta}$ < $Pr_{0.6}Sr_{0.4}CoO_{3-\delta}$ < $Gd_{0.6}Sr_{0.4}CoO_{3-\delta}$ < segukatoodid, kusjuures suurimad madalsagedusliku laenguülekande takistuse ja diffusioonilise takistuse väärtused tuvastati Ag + $La_{0.6}Sr_{0.4}CoO_{3-\delta}$ katoodimaterjali korral.

Aktivatsioonienergia väärtuste vähenemine seoses negatiivse polarisatsiooni suurenemisega ja laenguülekande koefitsiendi väärtused $\alpha_c > 0.5$ viitavad sellele, et lisaks laenguülekande protsessile on limiteerivaks ka elektro-

keemiliselt aktiivsete osakeste massiülekande protsess, mis on heas kooskõlas Nyquisti kõverate modelleerimisest saadud andmetega.

Poolelementide elektrokeemiliste parameetrite ajalise sõltuvuse andmed näitavad, et erinevad parameetrid ei sõltu ekspluatatsiooniajast või sõltuvad suhteliselt vähe. Mõnevõrra halvem elektrokeemiliste parameetrite stabiilsus tuvastati Ag-osakestega modifitseeritud katoodi korral, mis on ilmselt tingitud Ag-osakeste ümberstruktureerumisest katoodi pinnal pikaajalisel kuumutamisel.

10. ACKNOWLEDGEMENTS

I wish to express my greatest gratitude to my supervisors Professor Enn Lust and Gunnar Nurk for introducing and aiding me in electrochemistry, for valuable discussions and the patience in supervising me.

I would like to thank all my friends and colleagues for helpful discussions, inspirations and continuous support.

I wish to thank AS Elcogen and Estonian Science Foundation without whose financial help the work done would have been impossible to achieve.

Last but not least I want to thank my parents for patience and understanding over all these years.

11. PUBLICATIONS

I

E. Lust, **P. Möller**, I. Kivi, G. Nurk, S. Kallip, P. Nigu, K. Lust,
Optimization of the cathode composition for the intermediate-temperature SOFC.
Journal of the Electrochemical Society, 152 (2005) A2306–A2308.

II

E. Lust, G. Nurk, S. Kallip, I. Kivi, **P. Möller**,
Electrochemical characteristics
of $Ce_{0.8}Gd_{0.2}O_{1.9}|La_{0.6}Sr_{0.4}CoO_{3-\delta} + Ce_{0.8}Gd_{0.2}O_{1.9}$ half-cell.
Journal of Solid State Electrochemistry, 9 (2005) 674–683.

E. Lust, **P. Möller**, I. Kivi, G. Nurk, S. Kallip,
Electrochemical characteristics of $La_{0.6}Sr_{0.4}CoO_{3-\delta}$, $Pr_{0.6}Sr_{0.4}CoO_{3-\delta}$ and $Gd_{0.6}Sr_{0.4}CoO_{3-\delta}$ on $Ce_{0.85}Sm_{0.15}O_{1.925}$ electrolyte.
Journal of Solid State Electrochemistry, 9 (2005) 882–889.

IV

E. Lust, G. Nurk, **P. Möller**, I. Kivi, S. Kallip,
Oxygen reduction and electrochemical characteristics of half-cells
for intermediate SOFCs, 26th Risø International Symposium on
Materials Science, Risø, 2005, 279–284.

CURRICULUM VITAE

Priit Möller

Born:	05.07.1976, Laiuse, Estonia
Citizenship:	Estonian
Matrial status:	single
Address:	Institute of Chemistry University of Tartu 2 Jakobi St., Tartu 51014, Estonia
Phone:	+372 7 375 163
E-mail	priit.moller@ut.ee

Education

2001–2004	University of Tartu, Faculty of Physics and Chemistry, M.Sc in physical and electrochemistry, 2004
1994–2000	University of Tartu, Faculty of Physics and Chemistry, B. Sc. in chemistry, 2000

Professional employment

2004 – ...	University of Tartu, Institute of Physical Chemistry, researcher
2001–2004	University of Tartu, Institute of Physical Chemistry, chemist
2000–2001	Tartu Tehnoloogiad OY, chemist

List of publications

1. E. Lust, G. Nurk, A. Jänes, M. Arulepp, L. Permann, P. Nigu, P. Möller, Electrochemical properties of nanoporous carbon electrodes, Condensed Matter Physics 5 (2002) 307–327.
2. E. Lust, S. Kallip, P. Möller, A. Jänes, V. Sammelselg, P. Miidla, M. Väärtnõu, K. Lust, Influence of surface charge density on the electrochemically derived surface roughness of Bi electrodes, J. Electrochem. Soc. 150 (2003) E175–E184.
3. E. Lust, G. Nurk, A. Jänes, M. Arulepp, P. Nigu, P. Möller, S. Kallip, V. Sammelselg, Electrochemical properties of nanoporous carbon electrodes in various nonaqueous electrolytes. Journal of Solid State Electrochemistry, 7 (2003) 91–105.
4. R. Jager, E. Hark, P. Möller, J. Nerut, K. Lust, E. Lust, The kinetics of electroreduction of hexaamminecobalt(III) cation on Bi planes in aqueous

$HClO_4$ solutions. Journal of Electroanalytical Chemistry, 566 (2004) 217–226.
5. J. Nerut, P. Möller, E. Lust, Electroreduction of hexacyanoferrate(III) anions on electrochemically polished Cd(0001) plane. Electrochimica Acta, 49 (2004) 1597–1604.
6. E. Lust, G. Nurk, P. Möller, I. Kivi, S. Kallip, Oxygen reduction and electrochemical characteristics of half-cells for intermediate SOFCs, 26th Risø International Symposium on Materials Science, Risø, 2005, 279–284.
7. T. Thomberg, J. Nerut, R. Jager, P. Möller, K. Lust, E. Lust, The kinetics of electroreduction of peroxodisulfate ions on single crystal cadmium and bismuth electrodes. Journal of Electroanalytical Chemistry, 582 (2005) 130–143.
8. E. Lust, P. Möller, I. Kivi, G. Nurk, S. Kallip, P. Nigu, K. Lust, Optimization of the cathode composition for the intermediate-temperature SOFC. Journal of the Electrochemical Society, 152 (2005) A2306–A2308.
9. E. Lust, P. Möller, I. Kivi, G. Nurk, S. Kallip, Electrochemical characteristics of $La_{0.6}Sr_{0.4}CoO_{3-\delta}$, $Pr_{0.6}Sr_{0.4}CoO_{3-\delta}$ and $Gd_{0.6}Sr_{0.4}CoO_{3-\delta}$ on $Ce_{0.85}Sm_{0.15}O_{1.925}$ electrolyte. Journal of Solid State Electrochemistry, 9 (2005) 882–889.
10. E. Lust, G. Nurk, S. Kallip, I. Kivi, P. Möller, Electrochemical characteristics of $Ce_{0.8}Gd_{0.2}O_{1.9}|La_{0.6}Sr_{0.4}CoO_{3-\delta} + Ce_{0.8}Gd_{0.2}O_{1.9}$ half-cell. Journal of Solid State Electrochemistry, 9 (2005) 674–683.
11. Lust, E.; Möller, P.; Nurk, G.; Kivi, I.; Kallip, S. Influence of Electrode Porosity and Potential of the Oxygen Reduction Kinetics on the Intermediate Temperature SOFCs Cathodes . ECS Transactions 5 (2007) 423–434.
12. E. Lust, I. Kivi, G. Nurk, P. Möller, S. Kallip, V. Grozovski, H. Kurig, Influence of Cathode Porosity and Potential on Oxygen Reduction Kinetics at Intermediate Temperature SOFCs Cathodes. ECS Transactions 7 (2007) 1071–1080.
13. S. Kallip, H. Kasuk, V. Grozovski, P. Möller, E. Lust, Adsorption of camphor and 2,2′-bipyridine on Bi(111) electrode surface. Electrochimica Acta, (2007) 4035–4045.

ELULOOKIRJELDUS

Priit Möller

Sünniaeg ja koht:	05.07.1976, Laiuse, Eesti Vabariik
Kodakondsus:	Eesti
Prerekonnaseis:	vallaline
Aadress:	Keemia Instituut Tartu Ülikool Jakobi 2, Tartu 51014, Eesti
Telefon:	+372 7 375 163
E-post:	priit.moller@ut.ee

Haridus

2001–2004	Tartu Ülikool, füüsika-keemiateaduskond, M.Sc füüsikalise ja elektrokeemia erialal 2004
1994–2000	Tartu Ülikool, füüsika-keemiateaduskond, B.Sc kraad keemias 2000

Teenistuskäik

2004 – ...	Tartu Ülikool, Füüsikalise keemia instituut, teadur (0,5 k)
2001–2004	Tartu Ülikool, Füüsikalise keemia instituut, keemik
2000–2001	OÜ Tartu Tehnoloogiad, keemik

Ilmunud teaduspublikatsioonid

1. E. Lust, G. Nurk, A. Jänes, M. Arulepp, L. Permann, P. Nigu, P. Möller, Electrochemical properties of nanoporous carbon electrodes, Condensed Matter Physics 5 (2002) 307–327.
2. E. Lust, S. Kallip, P. Möller, A. Jänes, V. Sammelselg, P. Miidla, M. Väärtnõu, K. Lust, Influence of surface charge density on the electrochemically derived surface roughness of Bi electrodes, J. Electrochem. Soc. 150 (2003) E175–E184.
3. E. Lust, G. Nurk, A. Jänes, M. Arulepp, P. Nigu, P. Möller, S. Kallip, V. Sammelselg, Electrochemical properties of nanoporous carbon electrodes in various nonaqueous electrolytes. Journal of Solid State Electrochemistry, 7 (2003) 91–105.
4. R. Jager, E. Hark, P. Möller, J. Nerut, K. Lust, E. Lust, The kinetics of electroreduction of hexaamminecobalt(III) cation on Bi planes in aqueous

$HClO_4$ solutions. Journal of Electroanalytical Chemistry, 566 (2004) 217–226.
5. J. Nerut, P. Möller, E. Lust, Electroreduction of hexacyanoferrate(III) anions on electrochemically polished Cd(0001) plane. Electrochimica Acta, 49 (2004) 1597–1604.
6. E. Lust, G. Nurk, P. Möller, I. Kivi, S. Kallip, Oxygen reduction and electrochemical characteristics of half-cells for intermediate SOFCs, 26th Risø International Symposium on Materials Science, Risø, 2005, 279–284.
7. T. Thomberg, J. Nerut, R. Jager, P. Möller, K. Lust, E. Lust, The kinetics of electroreduction of peroxodisulfate ions on single crystal cadmium and bismuth electrodes. Journal of Electroanalytical Chemistry, 582 (2005) 130–143.
8. E. Lust, P. Möller, I. Kivi, G. Nurk, S. Kallip, P. Nigu, K. Lust, Optimization of the cathode composition for the intermediate-temperature SOFC. Journal of the Electrochemical Society, 152 (2005) A2306–A2308.
9. E. Lust, P. Möller, I. Kivi, G. Nurk, S. Kallip, Electrochemical characteristics of $La_{0.6}Sr_{0.4}CoO_{3-\delta}$, $Pr_{0.6}Sr_{0.4}CoO_{3-\delta}$ and $Gd_{0.6}Sr_{0.4}CoO_{3-\delta}$ on $Ce_{0.85}Sm_{0.15}O_{1.925}$ electrolyte. Journal of Solid State Electrochemistry, 9 (2005) 882–889.
10. E. Lust, G. Nurk, S. Kallip, I. Kivi, P. Möller, Electrochemical characteristics of $Ce_{0.8}Gd_{0.2}O_{1.9}|La_{0.6}Sr_{0.4}CoO_{3-\delta} + Ce_{0.8}Gd_{0.2}O_{1.9}$ half-cell. Journal of Solid State Electrochemistry, 9 (2005) 674–683.
11. Lust, E.; Möller, P.; Nurk, G.; Kivi, I.; Kallip, S. Influence of Electrode Porosity and Potential of the Oxygen Reduction Kinetics on the Intermediate Temperature SOFCs Cathodes . ECS Transactions 5 (2007) 423–434.
12. E. Lust, I. Kivi, G. Nurk, P. Möller, S. Kallip, V. Grozovski, H. Kurig, Influence of Cathode Porosity and Potential on Oxygen Reduction Kinetics at Intermediate Temperature SOFCs Cathodes. ECS Transactions 7 (2007) 1071–1080.
13. S. Kallip, H. Kasuk, V. Grozovski, P. Möller, E. Lust, Adsorption of camphor and 2,2′-bipyridine on Bi(111) electrode surface. Electrochimica Acta, (2007) 4035–4045.

DISSERTATIONES CHIMICAE UNIVERSITATIS TARTUENSIS

1. **Toomas Tamm.** Quantum-chemical simulation of solvent effects. Tartu, 1993, 110 p.
2. **Peeter Burk.** Theoretical study of gas-phase acid-base equilibria. Tartu, 1994, 96 p.
3. **Victor Lobanov.** Quantitative structure-property relationships in large descriptor spaces. Tartu, 1995, 135 p.
4. **Vahur Mäemets.** The ^{17}O and ^{1}H nuclear magnetic resonance study of H_2O in individual solvents and its charged clusters in aqueous solutions of electrolytes. Tartu, 1997, 140 p.
5. **Andrus Metsala.** Microcanonical rate constant in nonequilibrium distribution of vibrational energy and in restricted intramolecular vibrational energy redistribution on the basis of slater's theory of unimolecular reactions. Tartu, 1997, 150 p.
6. **Uko Maran.** Quantum-mechanical study of potential energy surfaces in different environments. Tartu, 1997, 137 p.
7. **Alar Jänes.** Adsorption of organic compounds on antimony, bismuth and cadmium electrodes. Tartu, 1998, 219 p.
8. **Kaido Tammeveski.** Oxygen electroreduction on thin platinum films and the electrochemical detection of superoxide anion. Tartu, 1998, 139 p.
9. **Ivo Leito.** Studies of Brønsted acid-base equilibria in water and non-aqueous media. Tartu, 1998, 101 p.
10. **Jaan Leis.** Conformational dynamics and equilibria in amides. Tartu, 1998, 131 p.
11. **Toonika Rinken.** The modelling of amperometric biosensors based on oxidoreductases. Tartu, 2000, 108 p.
12. **Dmitri Panov.** Partially solvated Grignard reagents. Tartu, 2000, 64 p.
13. **Kaja Orupõld.** Treatment and analysis of phenolic wastewater with microorganisms. Tartu, 2000, 123 p.
14. **Jüri Ivask.** Ion Chromatographic determination of major anions and cations in polar ice core. Tartu, 2000, 85 p.
15. **Lauri Vares.** Stereoselective Synthesis of Tetrahydrofuran and Tetrahydropyran Derivatives by Use of Asymmetric Horner-Wadsworth-Emmons and Ring Closure Reactions. Tartu, 2000, 184 p.
16. **Martin Lepiku.** Kinetic aspects of dopamine D_2 receptor interactions with specific ligands. Tartu, 2000, 81 p.
17. **Katrin Sak.** Some aspects of ligand specificity of P2Y receptors. Tartu, 2000, 106 p.
18. **Vello Pällin.** The role of solvation in the formation of iotsitch complexes. Tartu, 2001, 95 p.

19. **Katrin Kollist.** Interactions between polycyclic aromatic compounds and humic substances. Tartu, 2001, 93 p.
20. **Ivar Koppel.** Quantum chemical study of acidity of strong and superstrong Brønsted acids. Tartu, 2001, 104 p.
21. **Viljar Pihl.** The study of the substituent and solvent effects on the acidity of OH and CH acids. Tartu, 2001, 132 p.
22. **Natalia Palm.** Specification of the minimum, sufficient and significant set of descriptors for general description of solvent effects. Tartu, 2001, 134 p.
23. **Sulev Sild.** QSPR/QSAR approaches for complex molecular systems. Tartu, 2001, 134 p.
24. **Ruslan Petrukhin.** Industrial applications of the quantitative structure-property relationships. Tartu, 2001, 162 p.
25. **Boris V. Rogovoy.** Synthesis of (benzotriazolyl)carboximidamides and their application in relations with *N*- and *S*-nucleophyles. Tartu, 2002, 84 p.
26. **Koit Herodes.** Solvent effects on UV-vis absorption spectra of some solvatochromic substances in binary solvent mixtures: the preferential solvation model. Tartu, 2002, 102 p.
27. **Anti Perkson.** Synthesis and characterisation of nanostructured carbon. Tartu, 2002, 152 p.
28. **Ivari Kaljurand.** Self-consistent acidity scales of neutral and cationic Brønsted acids in acetonitrile and tetrahydrofuran. Tartu, 2003, 108 p.
29. **Karmen Lust.** Adsorption of anions on bismuth single crystal electrodes. Tartu, 2003, 128 p.
30. **Mare Piirsalu.** Substituent, temperature and solvent effects on the alkaline hydrolysis of substituted phenyl and alkyl esters of benzoic acid. Tartu, 2003, 156 p.
31. **Meeri Sassian.** Reactions of partially solvated Grignard reagents. Tartu, 2003, 78 p.
32. **Tarmo Tamm.** Quantum chemical modelling of polypyrrole. Tartu, 2003. 100 p.
33. **Erik Teinemaa.** The environmental fate of the particulate matter and organic pollutants from an oil shale power plant. Tartu, 2003. 102 p.
34. **Jaana Tammiku-Taul.** Quantum chemical study of the properties of Grignard reagents. Tartu, 2003. 120 p.
35. **Andre Lomaka.** Biomedical applications of predictive computational chemistry. Tartu, 2003. 132 p.
36. **Kostyantyn Kirichenko.** Benzotriazole — Mediated Carbon–Carbon Bond Formation. Tartu, 2003. 132 p.
37. **Gunnar Nurk.** Adsorption kinetics of some organic compounds on bismuth single crystal electrodes. Tartu, 2003, 170 p.
38. **Mati Arulepp.** Electrochemical characteristics of porous carbon materials and electrical double layer capacitors. Tartu, 2003, 196 p.

39. **Dan Cornel Fara.** QSPR modeling of complexation and distribution of organic compounds. Tartu, 2004, 126 p.
40. **Riina Mahlapuu.** Signalling of galanin and amyloid precursor protein through adenylate cyclase. Tartu, 2004, 124 p.
41. **Mihkel Kerikmäe.** Some luminescent materials for dosimetric applications and physical research. Tartu, 2004, 143 p.
42. **Jaanus Kruusma.** Determination of some important trace metal ions in human blood. Tartu, 2004, 115 p.
43. **Urmas Johanson.** Investigations of the electrochemical properties of polypyrrole modified electrodes. Tartu, 2004, 91 p.
44. **Kaido Sillar.** Computational study of the acid sites in zeolite ZSM-5. Tartu, 2004, 80 p.
45. **Aldo Oras.** Kinetic aspects of dATPαS interaction with $P2Y_1$ receptor. Tartu, 2004, 75 p.
46. **Erik Mölder.** Measurement of the oxygen mass transfer through the air-water interface. Tartu, 2005, 73 p.
47. **Thomas Thomberg.** The kinetics of electroreduction of peroxodisulfate anion on cadmium (0001) single crystal electrode. Tartu, 2005, 95 p.
48. **Olavi Loog.** Aspects of condensations of carbonyl compounds and their imine analogues. Tartu, 2005, 83 p.
49. **Siim Salmar.** Effect of ultrasound on ester hydrolysis in aqueous ethanol. Tartu, 2006, 73 p.
50. **Ain Uustare.** Modulation of signal transduction of heptahelical receptors by other receptors and G proteins. Tartu, 2006, 121 p.
51. **Sergei Yurchenko.** Determination of some carcinogenic contaminants in food. Tartu, 2006, 143 p.
52. **Kaido Tämm.** QSPR modeling of some properties of organic compounds. Tartu, 2006, 67 p.
53. **Olga Tšubrik.** New methods in the synthesis of multisubstituted hydrazines. Tartu. 2006, 183 p.
54. **Lilli Sooväli.** Spectrophotometric measurements and their uncertainty in chemical analysis and dissociation constant measurements. Tartu, 2006, 125 p.
55. **Eve Koort.** Uncertainty estimation of potentiometrically measured ph and pK_a values. Tartu, 2006, 139 p.
56. **Sergei Kopanchuk.** Regulation of ligand binding to melanocortin receptor subtypes. Tartu, 2006, 119 p.
57. **Silvar Kallip.** Surface structure of some bismuth and antimony single crystal electrodes. Tartu, 2006, 107 p.
58. **Kristjan Saal.** Surface silanization and its application in biomolecule coupling. Tartu, 2006, 77 p.
59. **Tanel Tätte.** High viscosity $Sn(OBu)_4$ oligomeric concentrates and their applications in technology. Tartu, 2006, 91 p.

60. **Dimitar Atanasov Dobchev**. Robust QSAR methods for the prediction of properties from molecular structure. Tartu, 2006, 118 p.
61. **Hannes Hagu**. Impact of ultrasound on hydrophobic interactions in solutions. Tartu, 2007, 81 p.
62. **Rutha Jäger.** Electroreduction of peroxodisulfate anion on bismuth electrodes. Tartu, 2007, 142 p.
63. **Kaido Viht.** Immobilizable bisubstrate-analogue inhibitors of basophilic protein kinases: development and application in biosensors. Tartu, 2007, 88 p.
64. **Eva-Ingrid Rõõm.** Acid-base equilibria in nonpolar media. Tartu, 2007, 156 p.
65. **Sven Tamp.** DFT study of the cesium cation containing complexes relevant to the cesium cation binding by the humic acids. Tartu, 2007, 102 p.
66. **Jaak Nerut.** Electroreduction of hexacyanoferrate(III) anion on Cadmium (0001) single crystal electrode. Tartu, 2007, 180 p.
67. **Lauri Jalukse.** Measurement uncertainty estimation in amperometric dissolved oxygen concentration measurement. Tartu, 2007, 112 p.
68. **Aime Lust.** Charge state of dopants and ordered clusters formation in CaF_2:Mn and CaF_2:Eu luminophors. Tartu, 2007, 100 p.
69. **Iiris Kahn**. Quantitative Structure-Activity Relationships of environmentally relevant properties. Tartu, 2007, 98 p.
70. **Mari Reinik.** Nitrates, nitrites, N-nitrosamines and polycyclic aromatic hydrocarbons in food: analytical methods, occurrence and dietary intake. Tartu, 2007, 172 p.
71. **Heili Kasuk.** Thermodynamic parameters and adsorption kinetics of organic compounds forming the compact adsorption layer at Bi single crystal electrodes. Tartu, 2007, 212 p.
72. **Erki Enkvist.** Synthesis of adenosine-peptide conjugates for biological applications. Tartu, 2007, 114 p.
73. **Svetoslav Hristov Slavov**. Biomedical applications of the QSAR approach. Tartu, 2007, 146 p.
74. **Eneli Härk.** Electroreduction of complex cations on electrochemically polished Bi(*hkl*) single crystal electrodes. Tartu, 2008, 158 p.